Sediment Transport by Released Anchor Ice: Field Measurements and Digital Image Processing

by

Hayden Edward Kalke

A thesis submitted in partial fulfillment of the requirements for the degree of

Master of Science

in

Water Resources Engineering

Department of Civil and Environmental Engineering
University of Alberta

Abstract

The importance of anchor ice transport of sediment on a river is significantly understudied. This study addresses the lack of data related to anchor ice release and rafting. A large sample set of anchor ice was collected in the field over the 2015-2016 and 2016-2017 winter seasons to compute a mean sediment concentration (± standard deviation) contained in anchor ice of 28.2 ± 33.2 g/L. Coarse sediment was also plucked from the top of passing anchor ice to better understand the mass and size of the largest sediment moved through this unique sediment transport process. The mean mass and major chord length of particles transported by anchor ice were 47.7 g and 3.6 cm, respectively. This indicated that a majority of the coarse sediment transported by anchor ice is gravel size. Additionally, it was found that 24% of the mass transported came from only 1.2% of the particles sampled. The sediment concentration, major chord length of coarse sediment, and mass of coarse sediment were all modelled reasonably well by a lognormal distribution.

The amount of sediment transported by anchor ice can be assessed if the measured sediment concentration in anchor ice pans discussed above is combined with the quantity of anchor ice released over the course of the winter. Digital images of surface ice, both frazil and anchor ice, were collected with bridge-mounted game cameras and an unmanned aerial vehicle (UAV). Algorithms to compute the quantity of frazil and anchor ice in the flow from the images were developed. Three site-specific learning models, support vector machines, were trained to produce binary images from raw digital images that separated the total surface ice from the

water. Another support vector machine model was also trained to then separate the predicted surface ice into the frazil and anchor ice components on the Peace River. These support vector machine models allowed for a variety of applications to be performed that improve our understanding of freeze-up processes. This included a spatial distribution of surface ice concentration with UAV acquired images, a time series of surface ice concentration leading to freeze-up with images acquired from bridge-mounted game cameras, and the computation of an instantaneous sediment mass flux during an anchor ice release event.

Preface

This thesis research is an original work by Hayden Edward Kalke under supervision of Dr. Mark Loewen in the Department of Civil and Environmental Engineering at the University of Alberta.

Chapter 2 of this thesis has been accepted for publication as "Kalke, H., McFarlane, V., Schneck, C., and Loewen, M. 2017. The transport of sediments by released anchor ice. Cold Regions Science and Technology." I was responsible for the field data collection, laboratory analysis, and the manuscript composition. McFarlane, V. and Schneck, C. assisted with the field data collection and contributed to manuscript edits. Loewen, M. was the supervisory author and was involved with concept formation and manuscript edits.

Chapter 3 of this thesis has been submitted to Cold Regions Science and Technology to be published as "Kalke, H. and Loewen, M. 2017. Support vector machine learning applied to digital images of river ice conditions." I was responsible for the field data collection, image processing, model training, and the manuscript composition. Loewen, M. was the supervisory author and was involved with concept formation and manuscript edits.

This thesis is dedicated to my loving girlfriend Marlyse and my dog Zoey.
Without whom none of my success would be possible.

Acknowledgments

The author would like to express his gratitude for the assistance and guidance provided by my supervisor Dr. Mark Loewen. The mentorship and time spent reviewing all aspects of this thesis are very much appreciated. Thank you to Dr. Nicholas Beier for being on the examining committee and Dr. Evan Davies for chairing the exam.

The author would like to thank David Zhao and Chen Liang for facilitating access to the laboratory at the University of Alberta. Thank you to Perry Fedun for his assistance with developing field apparatus used in this study. The author also thanks Christopher Schneck and Vincent McFarlane for all their assistance in the field and laboratory.

The author also thanks Professor Nilanjan Ray and Abhineet Singh from the Department of Computing Science at the University of Alberta for their assistance with the technical aspects of machine learning.

My deepest appreciation goes out to my girlfriend and best friend, Marlyse, for her love and support throughout my program.

This research was supported by the Natural Sciences and Engineering Research Council of Canada and is gratefully acknowledged.

Table of Contents

List of Tables

List of Figures

Chapter 1 Introduction

1.1 Background

River ice formation is a complex process that occurs on northern rivers during the winter season. This process begins when the river is exposed to prolonged freezing air temperatures that causes the water column to begin to supercool (i.e. water temperature drops below 0°C). As the water column is cooled below 0°C, frazil ice formation begins. Frazil ice growth begins through secondary nucleation that occurs on seed crystals introduced into the turbulent water column during supercooling (Daly, 1994). Figure 1-1 shows typical disc shaped frazil crystals and frazil flocs observed during supercooling. Seed crystals originate from water vapour that sublimates into ice crystals (Osterkamp, 1978), from an existing large ice crystal that sheds tiny ice fragments (Daly, 1994), or from small water droplets generated by breaking waves at the water surface (Gosink and Osterkamp, 1986). Frazil particles are inherently adhesive in nature (Kempema and Ettema, 2011) and as they are mixed in the turbulent flow they sinter together, forming larger frazil flocs. As frazil flocs grow in size, the buoyancy of the floc eventually causes it to rise to the surface forming surface slush. Figure 1-2 shows surface slush observed on the North Saskatchewan River during freeze-up. The surface slush (frazil flocs at the water surface) is exposed to freezing air temperatures as they move downstream, eventually forming solid frazil ice pans. Figure 1-3 shows frazil ice pans and larger rafts on the North Saskatchewan River later in the freeze-up process. As frazil pans collide with one another they become circular, pancake ice with upturned edges. Frazil pans have also been observed to freeze together to form larger frazil ice rafts, as seen in Figure 1-3.

Frazil ice crystals that are rapidly mixed in the flow may come into contact with the river bed and freeze there forming anchor ice. Anchor ice is immobile frazil ice frozen to a surface (i.e. river bed, trash rack) in the flow. Figure 1-4 shows a large in-place anchor ice accumulation observed on the Kananaskis River. The growth of

anchor ice occurs in three distinct stages: initial, transitional, and final growth stages (Kerr et al., 2002). Anchor ice growth has been observed to occur when the Froude number is between 0.2 and 1.0 (Hirayama et al., 1997; Terada et al., 1998). This growth begins with frazil deposition into the front-face, back-face, and contact points between gravel in the river substrate (Kerr et al., 1997; Qu and Doering, 2007; Stickler and Alfredsen, 2009). As more frazil is deposited in the transitional stage and the anchor ice formation begins to develop, it grows vertically towards the free surface. This increases the drag force experienced at the top of the accumulation, which can flatten or release the entire accumulation (Kerr et al., 2002). The final growth stage occurs once the anchor ice formation is flattened and becomes sufficiently dense to resist the drag force on the accumulation. During this final stage, growth can be driven by both frazil accumulation and in-situ crystal growth (Kempema and Ettema, 2011; Qu and Doering, 2007; Kempema et al., 2008). Kempema and Ettema (2011) concluded that frazil accumulation allows anchor ice to cover a large area of the river bed, whereas the internal strength and the strength of its bond to the bed is governed by its in-situ crystal growth.

Anchor ice release can occur mechanically or thermally and has been observed in both the laboratory and field (e.g. Kerr et al. 1997; Doering et al., 2001; Jasek et al. 2015; Tsang, 1982). Anchor ice is released when the bond between the formation and the substrate is overcome through a number of forces: pressure, shear, or buoyancy. Mechanical release occurs through the action of the drag force exerted by the flow acting against the accumulation, or by the inherent buoyancy of the formation. In a laboratory study by Kerr et al. (1997) anchor ice was observed to grow vertically until it was either released due to the increased drag force or was flattened and became sufficient dense to resist the increased drag force. It was noted that a sudden disturbance, i.e. when a portion of anchor ice released from the bed, could lead to the release the entire anchor ice formation. Another mechanical release mechanism that can occur is when the anchor formation grows sufficiently large that its internal buoyancy overcomes the bond to the substrate (e.g. Jasek et al. (2015)). Thermal release of anchor ice occurs when the water column is warmed

by incoming solar radiation thereby weakening the bond between the formation and the substrate to a point where the buoyancy is then able to lift the formation from the bed.

As anchor ice is lifted from the bed it carries entrapped bed material and "rafts" it downstream. Figure 1-5 shows a released anchor ice pan rafting both coarse and fine sediment on the Peace River. Rafted bed material is deposited downstream onto the bed or suspended into the flow. The deposition of bed material back into the flow can occur immediately as it is rafted downstream. However, if the anchor ice pan reaches the ice front it is incorporated into the solid ice cover and in this case the deposition of bed material would occur during the spring thaw. There have also been field observations of coarse sediment dropped on top of in-place anchor ice, which is then subsequently transported further downstream (Kempema and Ettema, 2011). This "leap-frogging" can significantly increase the distance coarse sediment is transported.

There are a number of studies that report observations of anchor ice transporting entrapped sediment in the field (Dayton et al., 1969; Jasek et al., 2015; Kempema et al., 2008; Kempema and Ettema, 2011; Stickler and Alfredsen, 2009; Terada et al., 1998; Tremblay et al., 2014; Tsang, 1982; Wigle, 1970; Yamazaki et al., 1996). However, field studies that directly measure the amount of sediment contained in released anchor ice are rare. Only one study has been conducted in the field that measures the sediment concentration in released anchor ice on rivers. Kempema and Ettema (2011) sampled anchor ice on the Laramie River in Wyoming and found a range of sediment concentrations from 0.37 to 108 g/L, with a mean sediment concentration (± standard deviation) of 22 ± 25 g/L. Kempema and Ettema (2011) concluded that more measurements of sediment in anchor ice need to be made over a wide range of scales to avoid scale inconsistencies. The contribution of sediment transported by anchor ice to a river's annual sediment budget is unknown. However, the impact of anchor ice rafting to a river's sediment budget may be significant. For example, Kempema and Ettema (2011) note that the coarsest

sediment on the Laramie River is transported by anchor ice rafting, not peak flows, and this occurs during winter low-flow in a period of minimum sediment transport.

1.2 Research Objectives

The objectives of this research are to improve our understanding of anchor ice rafting and its importance to the annual sediment budget of rivers. A first step in achieving these objectives is to address the lack of available field measurements of the sediment concentration in anchor ice pans. There has been only one previous study that reported measurements of sediment concentrations in released anchor ice and it was conducted on the Laramie River, where winter discharges are less than 1.2 m^3/s. Understanding the sediment contained in anchor ice on larger scale rivers, such as the Peace River where average winter discharge is roughly 1500 m^3/s will aid in our understanding of anchor ice rafting for a variety of river scales. Therefore, a large number of anchor ice samples were collected on the North Saskatchewan, Peace, and Kananaskis Rivers in Alberta in the winters of 2015-2016 and 2016-2017. The samples were analyzed in the laboratory and sediment concentrations were measured. In addition to this, coarse sediment was sampled by hand from the top of passing anchor ice pans to obtain a range of masses and major chord lengths. A detailed description of these field measurements is presented in Chapter 2.

The importance of anchor ice rafting to a river's annual sediment budget can be assessed if estimates of the quantity of anchor ice released over the course of the winter are combined with the sediment concentration measurements described above. One method for estimating the total volume or mass of surface ice being transported is to capture digital images of surface ice conditions on a river. Digital image processing algorithms can then be used to estimate the total surface ice concentration and if the average ice pan thickness is known the total mass of surface ice in each image can be computed. In order to estimate the mass of sediment being rafted by anchor ice, the digital image processing algorithm must also be able to detect which pans in an image are anchor ice and which are frazil ice.

In this study, the feasibility of using a support vector machine (SVM), a type of machine learning algorithm, to accurately compute the concentration of frazil and anchor ice pans was investigated. Digital images of surface ice conditions were acquired by a UAV and bridge-mounted game cameras during the winters of 2015-2016 and 2016-2017 on the North Saskatchewan and Peace Rivers. The SVM was first trained to analyze the raw digital images of surface ice conditions and produce a binary image in which the total surface ice (i.e. both frazil and anchor ice pans) and water were separated. Another SVM model was then trained to further separate the total surface ice into the frazil and anchor ice components. A detailed description of the model training and implementation is presented in Chapter 3.

Figures

Figure 1-1. Digital image showing typical disc shaped frazil particles and frazil flocs (image courtesy of V. McFarlane) (field of view is ~4.1 cm wide).

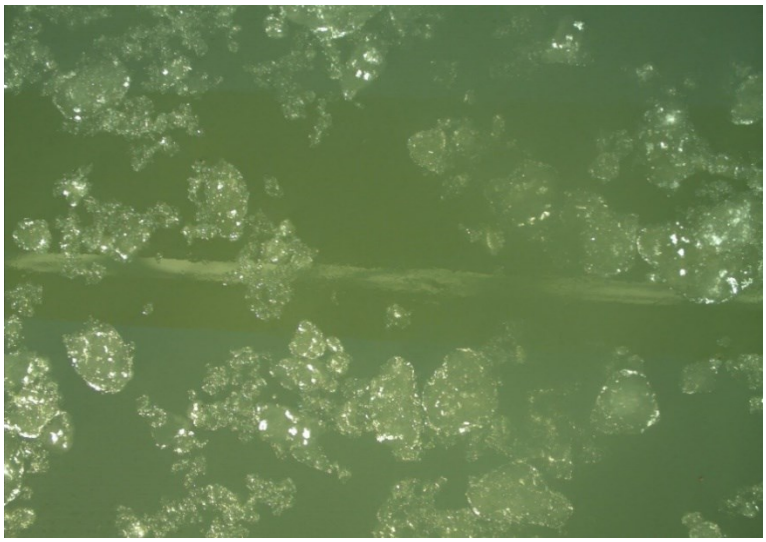

Figure 1-2. Digital image showing surface ice at the beginning of freeze-up on the North Saskatchewan River on November 24, 2016 (field of view is ~11 m wide).

Figure 1-3. Digital image taken on the North Saskatchewan River on December 3, 2016 showing frazil ice pans and larger frazil ice rafts (field of view is ~200 m wide).

Figure 1-4. Digital image showing a large anchor ice accumulation on the Kananaskis River on December 7, 2016.

Figure 1-5. Digital image showing an anchor ice pan rafting fine and coarse sediment on the Peace River on January 21, 2016.

References

Daly, S., 1994. Report on frazil ice. Hanover, New Hampshire.

Dayton, P.K., Robilliard, G., Devries, A.L., 1969. Anchor ice formation in McMurdo Sound, Antarctica. American Association for the Advancement of Science, Washington, D.C.

Gosink, J., Osterkamp, T., 1986. Frazil ice nucleation by ejecta from supercooled water, in: Proceedings of the 8th IAHR Symposium on Ice. Iowa City, Iowa, pp. 249–263.

Hirayama, K., Terada, K., Sato, M., Hirayama, K., Sasamoto, M., Yamazaki, M., 1997. Field measurements of anchor and frazil ice, in: Proceedings of the 9th Workshop on River Ice. Fredericton, NB.

Jasek, M., Shen, H.T., Pan, J., Paslawski, K., 2015. Anchor ice waves and their impact on winter ice cover stability, in: Proceedings of the 18th Workshop on the Hydraulics of Ice Covered Rivers. Quebec City, QC.

Kempema, E., Ettema, R., 2011. Anchor ice rafting: observations from the Laramie River. River Res. Appl. 27, 1126–1135.

Kempema, E., Ettema, R., McGee, B., 2008. Insights from anchor ice formation in the Laramie River, Wyoming, in: Proceedings of the 19th International Symposium on Ice. Vancouver, BC.

Kerr, D.J., Shen, H.T., Daly, S.F., 2002. Evolution and hydraulic resistance of anchor ice on gravel bed. Cold Reg. Sci. Technol. 35, 101–114.

Kerr, D.J., Shen, H.T., Daly, S.F., 1997. Anchor ice formation and growth on gravel channel bed, in: Proceedings of the 9th Workshop on River Ice. Fredericton, NB.

Osterkamp, T.E., 1978. Frazil Ice Formation: A Review. J. Hydraul. Div.

Qu, Y.X., Doering, J., 2007. Laboratory study of anchor ice evolution around rocks and on gravel beds. Can. J. Civ. Eng. 34, 46–55.

Stickler, M., Alfredsen, K., 2009. Anchor ice formation in streams: a field study. Hydrol. Process. 23, 2307–2315.

Terada, K., Hirayama, K., Sasamoto, M., 1998. Field Measurements of Anchor and

Frazil Ice, in: Proceedings of the 14th International Symposium on Ice. International Association for Hydro-Environment Envineering and Research, Potsdam, NY.

Tremblay, P., Leconte, R., Jay Lacey, R.W., Bergeron, N., 2014. Multi-day anchor ice cycles and bedload transport in a gravel-bed stream. J. Hydrol. 519, 364–375.

Tsang, G., 1982. Frazil and anchor ice: a monograph. NRC Subcommittee on Hydraulics of Ice Covered Rivers, Ottawa, ON.

Wigle, T.E., 1970. Investigations into frazil, bottom ice and surface ice formation in the Niagara River, in: Proceedings of the 1st International Symposium on Ice. International Association for Hydro-Environment Envineering and Research, Reykjavik, Iceland.

Yamazaki, M., Hirayama, K., Sakai, S., Sasamoto, M., Kiyohara, M., Takiguchi, H., 1996. Formation of frazil and anchor ice, in: Proceedings of the 13th International Symposium on Ice. International Association for Hydro-Environment Envineering and Research, Beijing, China.

Ye, S.Q., Doering, J., Shen, H.T., 2004. A laboratory study of frazil evolution in a counter- rotating flume. Can. J. Civ. Eng. 31, 899–914. doi:10.1139/L04-056

Chapter 2 The Transport of Sediments by Released Anchor Ice[1]

2.1 Introduction

The formation of anchor ice occurs annually on many northern rivers, where turbulent water is exposed to freezing air temperatures. Initially, small frazil crystals are generated and rapidly mixed in the water column as the temperature of the water drops below 0°C (i.e. the water column becomes supercooled). These frazil crystals are inherently adhesive or "sticky" in nature, and when they come in contact with the bed of a river due to the rapid mixing of the water column, they often freeze in place and begin to form anchor ice through continued frazil accumulation and/or in-situ growth (e.g. Kempema et al., 2008; Qu and Doering, 2007). Anchor ice formation has been observed to alter flow conditions in a river by altering bed roughness and shape (Kerr et al., 2002), and to transport sediment when it is released (Kalke et al., 2016, 2015; Kempema and Ettema, 2011).

Anchor ice formation is common downstream of a hydropower station because the release of warm water (>0°C) from the station inhibits ice formation and the river remains open downstream throughout the winter season. This enables frazil and, subsequently, anchor ice to form and release throughout the winter season. This is of interest given that extended periods of anchor ice formation and release alter a rivers winter ice regime. For example, Nafziger et al. (2017) observed different ice regimes between regulated and unregulated streams. It was observed that on regulated streams anchor ice events (formation and release) occurred throughout the winter season, whereas on unregulated streams anchor ice events were limited to before and after the establishment of a solid ice cover (Nafziger et al., 2017). It was also noted that on average the regulated streams experienced more anchor ice events than unregulated streams (Nafziger et al., 2017). Anchor ice formation in the

[1] This chapter has been published in Cold Regions Science and Technology as Kalke, H., McFarlane, V., Schneck, C., and Loewen, M. 2017. The transport of sediments by released anchor ice. Cold Reg. Sci. and Technol., 143, 70-80.

downstream reach can cause local staging at the tailrace that results in large operational losses for the station (e.g. Girling and Groeneveld, 1999). Anchor ice formed in the downstream reach will often release, either due to mechanical or thermal processes, which can impact downstream hydropower stations. For example, Jasek et al. (2015) reported that the release of anchor ice downstream of the W.A.C Bennett and Peace Canyon Dams caused large fluctuations (referred to as anchor ice waves) in water levels and discharge on the Peace River, Alberta. These fluctuations can result in flow restrictions (operational loss) from the dam while the ice cover is developing through the Town of Peace River. This is to ensure a stable ice cover forms and to prevent flooding during freeze-up or break-up (Jasek et al., 2015). Anchor ice releases downstream of the dams can also transport or "raft" sediment. On a regulated river, this could impact the overall sediment budget since anchor ice is formed and released frequently throughout a winter season. However, the overall impact of sediment transported by anchor ice is still unknown, and field studies that attempt to quantify the scale of sediment transported by anchor ice in rivers are rare.

There have been a few field studies that directly measured the sediment concentration in released anchor ice (Kalke et al., 2016, 2015; Kempema and Ettema, 2011). However, these studies had either small sample quantities (e.g. Kalke et al., 2016, 2015), or were performed on rivers with low winter discharge that may not be comparable to large rivers such as the Peace or North Saskatchewan River (e.g. Kempema and Ettema, 2011). In order to better estimate the impact of anchor ice rafting of sediment to the annual sediment budget downstream of a hydropower station, three regulated rivers were selected for anchor ice sampling in this study: the North Saskatchewan River, the Peace River, and the Kananaskis River. These samples provide data on the size range and concentrations of sediment contained in released anchor ice. This allows for better estimates of sediment transport when used in conjunction with anchor ice surface concentration obtained through digital images. In this study, grab samples of released anchor ice containing sediment were collected during the winters of 2015-2016 and 2016-2017.

Additionally, gravels and cobbles contained in released anchor ice were sampled to understand the impact of large bedload materials transported through anchor ice release.

2.2 Literature Review

2.2.1 Anchor Ice Formation

Anchor ice formation has been observed to grow in three distinct stages: initial, transitional, and final growth stages (Kerr et al., 2002). The initial stage of anchor ice growth has been observed in laboratory studies between Froude numbers of 0.14 and 0.76 (Doering et al., 2001; Kerr et al., 2002; Qu and Doering, 2007). Field observations of anchor ice growth have shown anchor ice formation to occur when the Froude number is between 0.2 and 1.0 (Hirayama et al., 1997; Terada et al., 1998). Anchor ice formation begins with frazil deposition on the front-face, back-face and contact points between gravel in the river bed substrate (Kerr et al., 1997; Qu and Doering, 2007; Stickler and Alfredsen, 2009). Figure 2-1 shows anchor ice formation on the front-face, back-face and contact points on the Kananaskis River. This deposited anchor ice grows quickly upwards towards the free surface with continued frazil deposition (Qu and Doering, 2007). As the anchor ice continues to grow above the crest of the gravel it begins to develop into three distinct forms: tail, scale, or ball-type formations depending on the Froude number (see Kerr et al. 2002). These small formations on individual gravel particles eventually come into contact with one another and form a continuous sheet of anchor ice. During the transitional stage, anchor ice continues to grows vertically towards the free surface, which increases the drag force on the accumulation; this either causes the anchor ice to flatten out or release (Kerr et al., 2002).

Once a sheet of anchor ice is flattened it can continue to grow through frazil accumulation or in-situ ice growth; this is the final growth stage. In-situ anchor ice growth is driven by heat and mass exchange between the anchor ice crystals and

the supercooled water (Kempema and Ettema, 2011). Kempema and Ettema (2011) concluded that an anchor ice accumulation could cover large areas of the river bed through continued frazil accumulation, whereas the internal strength of the anchor ice mass and the strength of its bond to the substrate came from its in-situ growth. Although anchor ice grows through both mechanisms, Kerr et al. (1997) observed no in-situ or dendritic growth occurring in the laboratory. This was attributed to the short time duration between successive frazil deposition and the negligible temperature difference between the anchor ice and supercooled water. Qu and Doering (2007) also observed in their laboratory experiments with a couette flow apparatus that frazil accumulation was the dominant mechanism of growth but noted that in-situ growth was also detected from the analysis of temperature curves but could not be detected in anchor ice images. Conversely, in a field study by Kempema et al. (2008) in-situ thermal growth was found to be the major contributor to the growth of anchor ice and frazil accumulation was not observed.

2.2.2 Anchor Ice Release and Rafting

Anchor ice release has been observed to occur through two mechanisms in the laboratory and field; mechanical or thermal release. Mechanical release occurs through the application of a mechanical force. This type of release can occur through the action of the shear force exerted by the flow acting against the anchor ice formation that causes it to release from the bed, or by the inherent buoyancy of the formation. Kerr et al. (1997) found in a laboratory study that when an anchor ice accumulation grew sufficiently thick, the increased drag caused the accumulation to either be released or flattened. As the anchor ice was flattened and the thickness was reduced, a sudden release of a section of the accumulation could cause a disturbance that released the entire anchor ice accumulation (Kerr et al., 1997). Doering et al., (2001) found that mechanical anchor ice release only occurred with a flow Reynolds number less than 42,000. Jasek et al. (2015) observed the mechanical release of an entire anchor ice formation in the Peace River. Another type of mechanical release occurs if the buoyant force acting on the

anchor ice exceeds the weight of the accumulation and the strength of the bond to the river bed.

Thermal release of anchor ice can occur when the water column warms above 0°C and causes a weakening of the ice-substrate bond (Tsang, 1982). Initially when the water column is supercooled, the bond between the anchor ice and the bed material is strong but as the water column begins to warm this bond is weakened (Tsang, 1982). Thermal release has been observed in the field to occur when the water column is warmed by solar radiation. Kempema and Ettema (2011) observed anchor ice releasing in the morning in the Laramie River in Wyoming when solar radiation warmed the water column and weakened the formation's bond to the bed until the buoyant force was able to lift the accumulation off the bed. Anchor ice releasing thermally was also observed by Jasek et al. (2015) on the Peace River when solar radiation caused the zero-degree isotherm to move downstream. Nafziger et al. (2017) observed anchor ice formation and release on one unregulated and two regulated streams in north-central New Brunswick. It was concluded that anchor ice release on these small streams was most strongly correlated to thermal factors (i.e. positive heat flux at the water surface and shortwave radiation). It was found that a positive heat flux at the water surface could predict complete anchor ice release on 93% of the days, and when coupled with air temperatures that exceeded -15°C this increased to 98% (Nafziger et al., 2017).

Regardless of the release mechanism, as the released anchor ice rises to the water surface it is capable of lifting entrapped bed material and transporting or "rafting" it downstream. A theoretical maximum sediment concentration that can be contained in neutrally buoyant anchor ice was found to be 122 g/L assuming the density of water, ice and sediment to be 1.0, 0.92 and 2.65 g/cm^3, respectively (Kempema et al., 1986). Rafted bed material can be deposited downstream onto the bed or on top of anchor ice accumulations if the anchor ice raft melts to the point where it can no longer hold the rafted sediment. Alternatively, rafted bed material may be transported downstream until it reaches the ice front and becomes frozen

into the ice cover. Eventually this sediment frozen into the ice cover will be suspended in the flow or deposited on the bed when the ice cover thaws in the spring.

2.2.3 Field Observations and Measurements of Anchor Ice Rafting

There have been a number of studies that report observations of sediment entrapped in released anchor ice in the field (Dayton et al., 1969; Jasek et al., 2015; Kempema et al., 2008; Kempema and Ettema, 2011; Stickler and Alfredsen, 2009; Terada et al., 1998; Tremblay et al., 2014; Tsang, 1982; Wigle, 1970; Yamazaki et al., 1996). However, field studies that quantify the amount of sediment rafted by anchor ice are relatively rare (Kalke et al., 2016, 2015; Kempema and Ettema, 2011; Kempema et al., 2001; Tremblay et al., 2014; Yamazaki et al., 1996).

Yamazaki et al. (1996) made observations of newly formed anchor ice on the Niuppu River in Hokkaido, Japan and found that the density of anchor ice increased with the velocity of flow. Anchor ice was observed to grow only in the rapid sections of the river and not observed in the milder sloped and deep flow sections or where the bed material was predominantly sand (Yamazaki et al., 1996). A large quantity of gravel was found on the surface of anchor ice accumulations and was assumed to be transported and dropped by other anchor ice as it floated by (Yamazaki et al., 1996). Figure 2-2 shows a similar observation in the Kananaskis River, where large gravels and cobbles were resting on an anchor ice accumulation. Samples of the gravel contained in the accumulations studied by Yamazaki et al. (1996) showed that they were only 0.4% to 0.7% of the weight of the anchor ice, and therefore would not have a dominant effect on the sediment transport during the winter season. A cobble of 30 cm in diameter was found inside an anchor ice mass, and at one site cobbles weighing 6 to 20 kg were contained in the ice ready to be transported (Yamazaki et al., 1996).

Kempema and Ettema (2011) made observations of anchor ice rafting and collected samples of anchor ice on the Laramie River. Anchor ice was observed to form most commonly on gravel and cobble substrates in riffles, but it was also observed to infrequently form on sand, and would release the following morning. Anchor-ice rafted cobbles weighing as much as 9.5 kg were observed in this study. A total of 32 anchor ice samples were collected using a dip net with the excess water drained off before returning to the laboratory and the sediment concentration ranged from 0.37 to 108 g/L, with a mean of 22 ± 25 g/L (± standard deviation). Kempema and Ettema (2011) concluded that anchor ice rafting was capable of transporting the largest bed material by size and weight and also transported more sediment compared to both bed and suspended load transport.

Kempema et al. (2001) observed anchor ice formation and rafting in the nearshore zone of southwestern Lake Michigan during the winter. Samples of released anchor ice and sediment laden ice remnants that rested on the sandy bed of the lake were collected. Sediment concentrations found in the 21 samples of released, floating anchor ice ranged from 1.2 to 102 g/L, with a mean concentration of 23.6 ± 26.4 g/L. A total of 4 samples of the sediment laden ice remnants were gathered from the lake bed and were found to have sediment concentrations ranging from 192 to 512 g/L.

Tremblay et al. (2014) studied particle movement due to anchor ice release by monitoring the movement of 104 sediment particles of similar grain size to the in-situ bed material in the Stoke River in Quebec. Each particle was equipped with a passive integrated transponder (PIT) that enabled its position to be monitored with the use of a mobile antenna and total station. Anchor ice formation and release was observed on seven occasions (three diurnal events and four multi-day events) during the winter of 2012-2013. Anchor ice rafting was observed to only occur after multiday growth of anchor ice. Diurnal anchor ice was small in extent (less than 0.05 m radius), translucent and never rafted any bed material. Tremblay et al. (2014) observed that 67 of the 104 particles tagged with PIT had moved, with 47

being theoretically too large to be moved by the flow. These anchor ice rafted cobbles weighed between 80 to 735 g and moved between 0.5 and 4 meters downstream of their initial position.

Wigle (1970) observed large masses of anchor ice on the Niagara River, Ontario. These masses ranged from a few centimeters to approximately a meter in diameter, rafting sediment (mainly sand and gravel) three to seven hours after sunrise. Dayton et al. (1969) observed anchor ice carrying portions of the stratum underneath the annual sea-ice cover upwards to the subice platelet layer; one observation noted a cobble that weighed at least 25 kg being rafted. Tsang (1982) observed on the Upper Niagara River that there was considerable deposition of large sediment particles in front of a hydraulic structure each spring. The Upper Niagara is not known for sediment transport, and it was concluded that the only possible mechanism capable of transporting particles of this size was rafting by anchor ice (Tsang, 1982). Stickler and Alfredsen (2009) took density measurements of anchor ice in three streams and found large rocks (< 3 kg) sitting on top of anchor ice, which indicated that they had been deposited there as released anchor ice passed overhead.

Kalke et al. (2015) computed instantaneous sediment mass fluxes due to anchor ice rafting for three events on the Peace River, AB in the winter of 2014-2015 and estimated that it ranged from 155 to 421 kg/s. This result was derived from two anchor ice samples with concentrations of 13 and 29 g/L and estimates of the frequency and duration of the three anchor ice events, the surface anchor ice concentration, and the thickness of anchor ice pans. Kalke et al. (2016) used an unmanned aerial vehicle to obtain digital images of the surface ice conditions and estimated total surface ice concentration and anchor ice pan concentration on the Peace River in the winter of 2015-2016. In that study the instantaneous sediment mass flux due to anchor ice rafting was estimated to range from 3 to 593 kg/s for three anchor ice release events.

2.3 Study Areas

Anchor ice rafting observations and sampling were conducted on three rivers in Alberta for this study: (1) North Saskatchewan River near Edmonton, (2) Peace River downstream of the W.A.C. Bennett Dam from the Dunvegan bridge to the Town of Peace River, and (3) Kananaskis River downstream of the Pocaterra Dam. Figure 2-3 shows a map of the study sites on all three rivers. Field measurements were collected on the Kananaskis River during the 2016-2017 winter, whereas measurements were collected on the North Saskatchewan and Peace Rivers during the 2015-2016 and 2016-2017 winters. Table 2-1 lists the location and coordinates for each anchor ice sampling event.

The North Saskatchewan River watershed drains an area of approximately 125,000 km^2 (Kellerhals et al., 1972) and is regulated by two dams, the Bighorn Dam (52°18'31"N 116°19'47"W) on the main reach and the Brazeau Dam (52°58'12"N 115°34'54"W) on the Brazeau River, which drains into the North Saskatchewan River. The combined flow from the Big Horn and Brazeau Dams is 111 m^3/s between October and March, based on daily average flow data from 1972-2012 compared to 126 m^3/s at the City of Edmonton. Therefore, approximately 90% of the flow in the City of Edmonton during the winter months originates from the Bighorn and Brazeau Dams. Anchor ice samples were collected during the 2015-2016 winter in the City of Edmonton at Emily Murphy Park. The anchor ice samples obtained from the North Saskatchewan River during the 2016-2017 winter were collected from three locations: (1) City of Edmonton at the Quesnell Bridge, (2) City of Edmonton at Emily Murphy Park, and (3) at the Genesee Bridge approximately one hour west of Edmonton. The Genesee, Quesnell, and Emily Murphy sampling locations are 354, 428, and 435 km downstream of the Bighorn Dam, and 189, 263, and 270 km downstream of the Brazeau Dam, respectively.

The Peace River drainage basin includes approximately 293,000 km^2 of northern British Columbia and Alberta, and is regulated by both the W.A.C. Bennett Dam

and Peace Canyon Dam (Church, 2015). Mean annual flow near the Town of Peace River located 357 km downstream of the W.A.C. Bennett Dam (WSC gauge 07HA001) is 1883 m^3/s post-regulation (Church, 2015). During the winter months, October to March, mean flow is approximately 1595 m^3/s near the Town of Peace River based on daily average flow data from 1972 to 2013. During the 2015-2016 winter anchor ice samples were collected at the Fairview water intake, at the Dunvegan Bridge boat launch, and on a boating expedition between these two sites. Anchor ice samples were collected at the Dunvegan Bridge boat launch and at the Shaftesbury Ferry crossing during the 2016-2017 winter. The Dunvegan Bridge boat launch, Fairview water intake and Shaftesbury Ferry crossing are located 296, 309, and 370 km downstream of the W.A.C. Bennett Dam, respectively.

The Kananaskis River is a tributary of the Bow River, and is located in southwestern Alberta. The study reach is located in the Canadian Rocky Mountains between the Pocaterra and Barrier Dams; this section of river is regulated and intense hydro-peaking typically occurs daily. This reach has a typical base flow of 0.5 m^3/s, with hydro-peaking flows of 23 m^3/s released from the Pocaterra Dam for up to six hours per day during the winter months (Emmer et al., 2013). Anchor ice samples were collected from the Kananaskis River 13 km downstream of the Pocaterra Dam near the Fortress Mountain Resort bridge in the 2016-2017 winter.

2.4 Methodology

2.4.1 Anchor Ice Sampling

Anchor ice samples were obtained from each river by wading into the river from the bank or working off the border ice (dependent on water levels), breaking off a portion of a released anchor ice pan with an ice scoop, and allowing any pore water to drain before placing it into a sealable plastic bag. A single anchor sample was taken from each pan. Anchor ice pans typically contained coarser sediment on the top of the pan and finer sediment dispersed homogeneously. Anchor ice sampling

was typically restricted to water depths less than ~1.0 m in all three rivers. Sampling was restricted to within 20 m of the bank in the North Saskatchewan River and in the Peace River, sampling was done directly from the border ice or within several meters of the edge of the border ice. The Kananaskis River was shallow enough that anchor ice samples were taken across the entire channel. Anchor ice samples had an average volume of 2.4 L, with ~80% of samples having volumes between one and three liters. Figure 2-4 shows the ice scoop used to capture and drain anchor ice samples. The collected samples were then returned to the University of Alberta to be analyzed for inorganic (total fixed solids) and organic (total volatile solids) solids per volume of melted ice (in units of g/L).

Anchor ice sampling on the North Saskatchewan River occurred on November 11, 2015, November 24 to 28, 2016, and December 3, 2016 (see Table 2-1). Samples collected at all sites on the North Saskatchewan River were sampled by wading into the river from the right bank. These samples are a combination of both manually and naturally released anchor ice. Samples were manually released by having one person walk through a large accumulation upstream and sampling the released, floating anchor ice downstream with the ice scoop. Walking through an accumulation typically caused a small quantity of anchor ice to release from the bed typically producing several anchor ice pans. This method was used at the Quesnell and Emily Murphy sites in the early stages of freeze-up when little to no anchor ice was releasing. At the Genesee site, all samples were released by natural means and collected as they moved through the sampling area near the right bank. Figure 2-5 shows an image of a visibly dirty anchor ice pan containing a range of sediment sizes (fine silts to large cobbles) that were being rafted on the North Saskatchewan River at Genesee.

On the Peace River, anchor ice samples from the winter of 2015-2016 included samples on January 23 and February 23, 2016 from the border ice at the Dunvegan Bridge boat launch on the right bank, and on January 14 and February 21, 2016 at the Fairview water intake by wading in from the border ice on the left bank.

Samples were also taken from a boat in water depths greater than one meter while floating between the Dunvegan Bridge and the Fairview Intake on January 21, 2016. Note that the three samples taken on January 14, 2016 had significantly larger volumes (20.6, 43.5, and 57.0 L) than any other collected samples. During the winter of 2016-2017, anchor ice samples were collected on January 14 and 15, 2017 from the border ice at the Dunvegan Bridge boat launch on the right bank, and on January 15, 2017 at the Shaftesbury Ferry crossing by wading in from the border ice on the left bank. All samples from the Peace River were taken from naturally released anchor ice pans.

Anchor ice samples from the Kananaskis River were collected on December 7 and 8, 2016. Anchor ice on the Kananaskis River releases very rapidly during the intense hydropeaking period (typically 8:00 PM to 12:00 AM at the Fortress site), and wading into the river to collect samples at these times was deemed unsafe. Manually releasing samples and allowing them to float downstream to be collected was not possible at this site since flow rates over the anchor ice weirs were quite high, making collection difficult. Therefore, samples were removed directly from anchor ice weirs and accumulations with the ice scoop and allowed to drain before being placed into a sealable bag. No released anchor ice was observed at the base flow; however, it was noted that the anchor ice weirs observed each day were newly formed in different locations. These samples were assumed to be representative of what would release during hydro-peaking events.

2.4.2 Sample Analysis

The total volume and mass of solids contained in anchor ice were analyzed in the laboratory to determine the total solids per unit volume of melted ice (g/L). The total solids were then separated into organic (total volatile solids) and inorganic (total fixed solids) fractions per unit volume of melted ice (g/L) by burning off organic material in a furnace.

First, the volume of each sample was measured by submerging the opened sample bag, containing the melted anchor ice sample, into a bucket completely filled with water and measuring the overflow volume. Preliminary tests with sample bags containing known volumes of water showed that this method of measuring the volume was accurate to ±5%. The sediment contained in each sample was comprised of two components: (1) the fine suspended sediment contained in the melt water and (2) the coarser settled sediment. A 100 ml subsample of the melt water was collected from each sample bag in order to measure the mass of suspended sediment. The excess water was then carefully drained from the sample leaving only the settled material and a small amount of water in the sample bag. This sample splitting greatly reduced the total volume of samples that needed to be transported back to the laboratory.

In the laboratory, the 100 ml subsample of melt water from each anchor ice sample was vacuum filtered through a Whatman Binder-Free Glass Microfiber Filter, Grade 943-AH, and placed into an aluminum tin; the filter and tin were oven dried at 105°C and weighed prior to filtering. The settled material was transferred into a separate aluminum tin of known mass. The aluminum tins were then placed into an evaporating oven at 105°C for one day, and then a furnace at 550°C for one hour to burn off any organic material. The tins were weighed after removal from each successive oven to determine the total solids (after 105°C) and the total fixed solids (after 550°C). The equations for calculating the total solids (*TS*) and total fixed solids (*TFS*) in g/L from the measured masses are as follows,

$$TS = \frac{m_{set,105} + m_{sus,105}}{V} \tag{2.1}$$

$$TFS = \frac{m_{set,550} + m_{sus,550}}{V} \tag{2.2}$$

where, $m_{sus,\ 105}$ and $m_{sus,550}$ are the mass of suspended material after drying in the oven and burning in the furnace, respectively, $m_{set,105}$ and $m_{set,550}$ are the mass of settled material after drying in the oven and burning in the furnace, respectively, and V is the total volume of the melted anchor ice sample. The mass of suspended material measured from the 100mL subsample is converted into a concentration (g/L) and then a total mass of suspended material can be calculated for the entire volume. The total volatile solids (TVS) was then computed by subtracting the total fixed solids from the total solids. The total fixed solids (g/L) is reported as the sediment concentration in anchor ice samples henceforth, since it only includes inorganic material contained within the anchor ice.

2.4.3 Sieve Analysis

The settled material from anchor ice samples was combined into three aggregate samples after burning at 550°C and were then sieved in the laboratory using the 1½", 1", ¾", ½", ⅜", No. 4, No. 10, No. 20, No. 40, No. 60, and No. 100 sieves. Samples were amalgamated since individual samples contained an insufficient quantity of sediment to obtain an accurate grain size distribution. The three aggregate samples were created by combining: (1) the 79 Peace River anchor ice samples collected on January 14 and 15, 2017, (2) the 114 North Saskatchewan and Kananaskis samples collected in the winter of 2016-2017, and (3) the three large Peace River samples collected on January 14, 2016. The sieves were shaken for 15 minutes, and then the mass of sediment retained on each sieve was measured. Note that the decision to perform the sieve analysis was made after the North Saskatchewan and Kananaskis samples had been combined, therefore they were sieved as one aggregate sample.

2.4.4 Gravel and Cobble Sampling

Gravels and cobbles were also sampled from released anchor ice to determine the range of sizes that are capable of being lifted from the bed by anchor ice. Samples

were obtained by wading in or working from the border ice and manually removing rocks from the surface of anchor ice pans as they floated by or by removing the anchor ice pans from the flow and sampling rocks contained in the entire pan. This type of sampling is referred to as "particle sampling" henceforth. This sampling included particles that were practical to sample by hand; this resulted in particles with diameters greater than approximately 0.6 cm. Particle sampling was typically conducted at a site for roughly 30 to 45 minutes. Sampling of particles contained in released anchor ice rafts occurred on November 26 and 27, 2016 at Emily Murphy Park; December 3, 2016 at Genesee; January 14, 2017 at the Dunvegan boat launch; and January 15, 2016 at the Shaftesbury Ferry crossing. On the Kananaskis River, no particle sampling was performed since anchor ice released when flow rates were too high to safely wade into the river. Additionally, masses and major chord lengths for similarly sized particles (i.e. larger than 0.6 cm in major chord length) contained in collected anchor ice samples were also measured. These two data sets are referred to as gravel and cobble sized rocks from particle sampling and from anchor ice sampling, henceforth.

Major chord lengths were measured by placing all particles obtained through particle sampling on a white board with an adjacent ruler for scale, taking a photograph and processing the digital image using MATLAB. This was performed by simple colour thresholding to convert the image into binary which was then compared to the original image and manually corrected if necessary using photo processing software, GIMP (GNU Image Manipulation Program) 2.0. This mainly involved removing shadows or filling in some particles that were identical to the background colour and did not threshold well in MATLAB. The extreme boundary points of each particle were found with the *regionprops* function in MATLAB, and the scale was calculated using the ruler placed on the white board. The major chord length of each particle was then determined by calculating the maximum distance between any two boundary points. The major chord lengths of particles contained in the anchor ice samples were measured by hand with a ruler.

2.4.5 Unmanned Aerial Vehicle Observations

An unmanned aerial vehicle (UAV) with a high resolution digital camera pointing downwards at the water surface was used to obtain images of ice conditions. The UAV was a Blade Chroma model equipped with a stabilized CGO3 4K camera, with both image capture and video recording capabilities, and was flown at all sampling sites except Emily Murphy and Quesnell. The digital images were used to collect qualitative information on anchor ice accumulations and release events. Site visits on the Peace River during the 2016-2017 winter occurred when anchor ice was releasing due to warm air temperatures. As a result the surface ice was comprised largely of released anchor ice with some broken ice as shown in the image presented in Figure 2-6. As discussed previously no anchor ice releases or rafting were observed during site visits on the Kananaskis River; however, multiple large anchor ice weirs were observed and the location and size of the weirs changed daily. Figure 2-7 shows of one of these large anchor ice weirs observed on the Kananaskis River.

2.5 Results

2.5.1 Anchor Ice

Table 2-2 summarizes the data from the analysis of anchor ice samples collected in the winters of 2015-2016 and 2016-2017. The measured range of total fixed solids in released anchor ice was fairly consistent between all three rivers, with ranges of 0.3 to 242.0 g/L, 0.6 to 147.2 g/L, and 0.3 to 140.1 g/L for the North Saskatchewan, Peace, and Kananaskis Rivers, respectively. The North Saskatchewan River samples contained two outliers with concentrations above 200 g/L; these were likely samples with large cobbles. The total volatile solids ranged from 0 to 5.03 g/L, and this corresponds on average to only 2.2% of the total solids. The low quantity of volatile solids found in the anchor ice samples shows that the material being rafted is predominantly inorganic sediment.

Mean sediment concentration results listed by river and winter season are presented in Table 2-3. It should be noted that although the standard deviation is larger than the mean in some cases, this does not imply that negative values of sediment concentration are possible. The mean sediment concentrations in Table 2-3 range from 11.9 to 37.7 g/L and the mean value for all anchor ice samples collected in both winters is 29.6 g/L. The coefficient of variation for the data listed in Table 2-3 ranged from 0.66 to 1.5 with an average value of 1.0 indicating that on average the standard deviation and the mean were approximately equal. The mean sediment concentrations from the winter seasons of 2015-2016 and 2016-2017 were 25.0 ± 25.3 g/L and 30.7 ± 35.0 g/L, respectively. The minimum value of 11.9 g/L was computed from only four samples collected on the North Saskatchewan River in 2015-2106 which is an extremely small sample size. The maximum value of 37.7 g/L was for the Kananaskis River samples that were collected directly from anchor ice weirs and accumulations and this may explain the higher concentrations. Eliminating the two extreme values the range of mean sediment concentrations presented in Table 2-3 is considerably smaller, 25.0 to 30.7 g/L. In Figure 2-8 a histogram is plotted of the sediment concentrations measured in all 239 anchor ice samples taken during the two winters and a lognormal distribution is a reasonable fit to the data.

2.5.2 Particle Sizes

A total of 1,470 gravel and cobble sized particles were sampled by hand from anchor ice pans during particle sampling in the North Saskatchewan and Peace River during the 2016-2017 winter. The masses of collected particles ranged from 0.2 g to 2106.6 g with a mean, median and standard deviation of 47.7 g, 15.4 g, and 126.5 g, respectively. A total of 244 particles were found in the collected anchor ice samples during the winter of 2016-2017. The mass of particles contained in the anchor ice samples had a mean, median and standard deviation of 23.8 g, 8.9 g, and 41.7 g, respectively. In Figure 2-9, histograms of the mass of the 244 particles found

in the 193 anchor ice samples collected during the 2016-2017 winter season and of the mass of the 1,470 gravel and cobble sized particles collected during particle sampling are compared. Approximately half of the total mass of all coarse sediment sampled during particle sampling was contained in particles that weigh less than 130 g. In addition, 24% of the total mass of particles sampled by hand was comprised of particles greater than 500g in mass.

The mean, median and standard deviation of the major chord length of the 1,470 gravel and cobble sized particles collected through particle sampling were 3.6, 3.2, and 2.1 cm, respectively. The mean, median and standard deviation of the major chord length of the 244 particles contained in collected anchor ice samples were 2.9, 2.5, and 1.6 cm, respectively. Figure 2-10 compares histograms of the major chord length of particles collected during particle sampling and those contained within anchor ice samples. A lognormal distribution was once again found to be representative of the data.

A plot of cumulative percent retained on the sieve for the three aggregate samples is shown in Figure 2-11. Table 2-4 summarizes the mass retained on each sieve for each sample. The cumulative percent retained plot for each of the three aggregate samples is relatively flat between grain sizes of 0.85 and 9.51 mm. Mass retained in this range was 3.6%, 8.3%, and 7.8% for the North Saskatchewan-Kananaskis River (NSR-KR) 2016/17 aggregate sample, the Peace River 2016/17 aggregate sample, and the Peace River January 14, 2016 aggregate sample, respectively. The North Saskatchewan-Kananaskis River and the Peace River January 14, 2016 aggregate samples had significantly more coarse sediment than the Peace River 2016/17 aggregate samples. It was determined that 55.6% and 64.3% of the total sediment in the North Saskatchewan-Kananaskis River and the Peace River January 14, 2016 aggregate samples, respectively, had grain sizes larger than 25mm, whereas the Peace River 2016/17 aggregate sample only had 9.7% of the total sediment coarser than 25mm. This could be due to differences in the size of the

local bed material or could be due to differences in the anchor ice release mechanism, i.e. thermal vs mechanical release.

2.6 Discussion

Samples collected from the same river but at locations separated by more than a few kilometers had sediment concentrations that varied considerably and this may be due to differences in the properties of the bed material at the different sites. For example, samples collected at Genesee had a mean sediment concentration ~50% larger than the samples collected in the City of Edmonton (i.e. 36.6 g/L compared to 24.3 g/L) located ~80 km downstream from Genesee. Samples collected at the Fairview, Dunvegan, and Shaftesbury sites on the Peace River had mean sediment concentrations of 15.5, 26.3 and 35.2 g/L, respectively. These sites are located 296, 309 and 370 km downstream of the W.A.C. Bennett Dam, respectively.

The mean sediment concentration found in anchor ice during both winter seasons on the North Saskatchewan, Peace and Kananaskis Rivers were 28.1, 28.3, and 37.7 g/L, respectively, with samples sizes of 83, 121, and 35, respectively. The samples collected from the Kananaskis River contained higher concentrations than either the North Saskatchewan or Peace Rivers. This could be a result of collecting samples from anchor ice weirs rather than collecting released anchor ice. The reason anchor ice sampled directly from these dams had higher sediment concentrations than released pans could be because sediment may be lost as pans are released and when they are advecting downstream. Another possible explanation is that anchor ice sediment concentration could be a function of the grain size of the bed material at the location where the accumulation formed. However, since no samples of bed material were gathered during this study no definitive conclusions can be drawn regarding the influence of local bed material properties.

Therefore, it was decided that an estimate of the mean sediment concentration in released anchor ice should be computed by excluding the samples taken from anchor ice weirs on the Kananaskis River. The 204 samples of released anchor ice taken on the North Saskatchewan and Peace Rivers had sediment concentrations that ranged from 0.2 to 241.95 g/L, with a mean concentration of 28.2 ± 33.2 g/L. By comparison Kempema and Ettema (2011) collected 32 released anchor ice samples on the Laramie River and found sediment concentrations ranging from 0.37 to 108 g/L, with a mean concentration of 22 ± 25 g/L.

Theoretically, the sediment concentration in floating anchor ice cannot exceed 122 g/L (Kempema et al., 1993), however 6 samples in this study were found with concentrations exceeding this limit. In this study most anchor ice samples were collected by sampling a small portion of a larger anchor ice pan and as result the concentration of the small sample could exceed 122 g/L while the concentration averaged over the entire pan was less than this limit. Three entire released anchor ice pans were collected on January 14, 2016 and were found to have concentrations of 19.0, 20.5, and 26.1 g/L which are close to the mean concentration observed in this study and the value reported by Kempema and Ettema (2011). This indicates that the sampling strategy employed in this study of sub-sampling a large number of anchor ice pans provides a representative dataset.

It has been observed previously in the laboratory that suspended frazil ice can also entrap suspended sediment and transport it. In a laboratory study conducted by Kempema et al. (1993) frazil and anchor ice were produced in a racetrack flume with two different beds comprised of well-sorted sand with a mean grain size of 0.25 and 0.30 mm in fresh and salt water. Sediment concentrations in sampled frazil ice ranged from 0.02 to 20.2 g/L, with a mean and standard deviation of 5.0 and 6.9 g/L, respectively. The sediment concentrations in anchor ice ranged from 1.04 to 88.3 g/L, with a mean and standard deviation of 28.3 and 29.1 g/L, respectively. Suspended sediment concentrations in the water were considerably smaller, with a mean and a standard deviation of 0.42 and 0.38 g/L, respectively. Sediment

concentration in frazil ice was also measured in another laboratory experiment conducted by Smedsrud (2001). In this study, frazil was generated in a tank containing suspended sediment with a maximum recorded sediment concentration of 0.199 g/L. Smedsrud (2001) found that sediment concentrations in surface slush were equivalent to that suspended in the water, and the maximum sediment concentration measured in frazil ice slush was 0.163 g/L. These laboratory measurements of sediment entrapped by frazil ice indicate that it is possible that not all of the sediment found in floating ice pans is contained in released anchor ice; a small fraction of it may be sediment that was entrapped by suspended frazil ice. It is important to distinguish between sediment that is rafted by anchor ice pans and that which is entrapped in suspended frazil. This is because in rivers with negligible bed loads, rafting by anchor ice is the only mechanism capable of transporting coarser sediment. As a result this mechanism may contribute significantly to the annual sediment budget of a river. The sediment entrapped in suspended frazil is finer suspended sediment that was already being transported downstream by the turbulent flow, therefore this mechanism will likely have very little impact on the annual sediment budget. However, field measurements of sediment concentrations found in frazil ice pans will be needed to determine how this mechanism contributes to the annual sediment budget.

The results from the sieve analysis of the aggregate samples plotted in Figure 2-11 show that two of the aggregate samples were much coarser than the third. The Peace River January 14, 2016 aggregate sample and the North Saskatchewan-Kananaskis Rivers 2016-2017 aggregate sample both had ~70% of the sediment larger than 9.51 mm. By comparison, the Peace River 2016-2017 aggregate sample had only 13% of the sediment larger than 9.51 mm. One possible explanation for this difference may be the mechanism responsible for anchor ice release. Peace River air temperatures remained below -13°C throughout the day on January 14, 2016, whereas on January 14-15, 2017 air temperatures were as high as 5°C and stayed above 0°C for most of the night. This suggests that the anchor ice event on January 14, 2016 was likely caused by mechanical release and the January 14-15, 2017

event by thermal release. However, air temperatures on the sampling dates when the aggregate North Saskatchewan-Kananaskis Rivers sample was collected did not conclusively indicate that thermal or mechanical release was the dominant mechanism. Note that another possible explanation for the disparity in the sediment size distributions in Figure 2-11 would be variations in the size of the bed material at the locations where the anchor ice accumulated. Additional field measurements will be required before the impact that the release mechanism has on the properties of the rafted sediments can be determined conclusively.

Perhaps the most interesting aspect of Figure 2-11 is the fact that all three curves are relatively flat for grain sizes from 1 mm to 9.51 mm. All three curves then increase dramatically at grain sizes smaller than 1 mm. This indicates that the aggregate samples were comprised largely of either very coarse particles, greater than 9.51 mm in size, or finer particles 1 mm or smaller in size. A plausible explanation for this is that very coarse particles (i.e. larger than 9.51 mm) are surrounded by anchor ice as it accumulates on the river bed and eventually become completely engulfed. However, intermediate size particles (i.e. between 0.85 mm and 9.51 mm) are perhaps small enough that they are not easily trapped inside anchor ice accumulations. The fine sediment particles may become trapped in the anchor ice in a completely different manner. There appears to be three modes of sediment entrapment into anchor ice masses: (1) coarse sediment incorporated into the bottom of the growing anchor ice mass, (2) fine-grained bed or suspended load sediment incorporated throughout the mass, and (3) sediment released from the bottom of an anchor ice pan that is deposited on top of in-place, growing anchor ice. The image in Figure 2-2 shows an anchor ice accumulation with finer sediment dispersed throughout the mass likely via mode (2) and coarse material deposited on top of the still in-place, growing mass likely via mode (3). Another explanation for observing little to no particles between 0.85 mm and 9.51 mm could be that these particles were also absent in the bed material and therefore would not be present in the anchor ice samples. Acquiring bed samples in future field studies could provide further insight as to why this size range is absent in anchor ice.

The instantaneous mass fluxes presented in Kalke et al. (2016) ranged from 3 to 593 kg/s and these estimates change to 0.4 to 1109 kg/s using the range of measured sediment concentration in anchor ice found in this study. In Kalke et al. (2016) the average instantaneous sediment mass flux was estimated to be 167 kg/s and 72 kg/s on January 21, 2016 and January 23, 2016, respectively. These preliminary estimates were computed using sediment concentration data from only eight anchor ice samples taken on January 21 and 23, 2016 with an average sediment concentration of 37 g/L. Using the average sediment concentration of 28.2 g/L obtained in this study, these instantaneous mass flux are reduced to 129 kg/s and 55 kg/s.

2.7 Conclusion

The sediment concentration contained in anchor ice on three very different Alberta rivers was investigated by collecting a total of 239 anchor ice samples. The mean, median and standard deviation of the sediment concentration in 204 floating anchor ice samples was found to be 28.2, 18.4, and 33.2 g/L, respectively. These concentrations are comparable to those reported in previous studies on the Laramie River (Kempema and Ettema, 2011) and on Lake Michigan (Kempema et al., 2001). Using the mean sediment concentration of 28.2 g/L determined in this study the instantaneous mass fluxes estimated by Kalke et al. (2016) are reduced by ~25% to 129 and 55 kg/s on January 21 and 23, 2016, respectively. The mean major chord length and mean mass of the 1,470 coarse particles sampled from floating anchor ice were 3.6 cm and 47.7 g, respectively. This indicates that a majority of the coarse sediment transported by anchor ice is gravel sized. It was also found during the gravel and cobble sampling that 1.2% of the particles (18 of 1,470) had a mass exceeding 500 g and these accounted for 24% of the total mass. The only mechanism capable of transporting these large cobble sized rocks is likely anchor ice rafting; the same conclusion reached by Kempema and Ettema (2011) in their Laramie River study. Sediment concentration, major chord length of coarse

sediment and mass of coarse sediment in anchor ice were all modelled reasonably well by a lognormal distribution. This study provides a better understanding of the sediment sizes and concentrations contained in released anchor ice pans and may ultimately lead to better predictions of the contribution of anchor ice transported sediment to a river's annual sediment budget. However, this will require future field studies to quantify the frequency and duration of anchor ice release events, the average thickness of released anchor ice, and anchor ice surface concentration during these events.

Acknowledgements

This research was supported by the Natural Sciences and Engineering Research Council of Canada (NSERC). We would like to thank Kerry Paslawski of Timberoot Environmental Inc., and Martin Jasek of BC Hydro for their help in acquiring anchor ice samples on the Peace River. We would also like to thank David Zhao and Chen Liang for facilitating access to the laboratory at the University of Alberta. The authors would like to thank the four anonymous reviewers whose comments helped improve and clarify this manuscript. Maps contained in this publication were produced using QGIS software (QGIS Development Team, 2017) using © OpenStreetMap data contributors (http://www.osm.org/copyright) and data obtained from AltaLIS (2017) which contains information licensed under the Open Government License – Alberta.

Figures

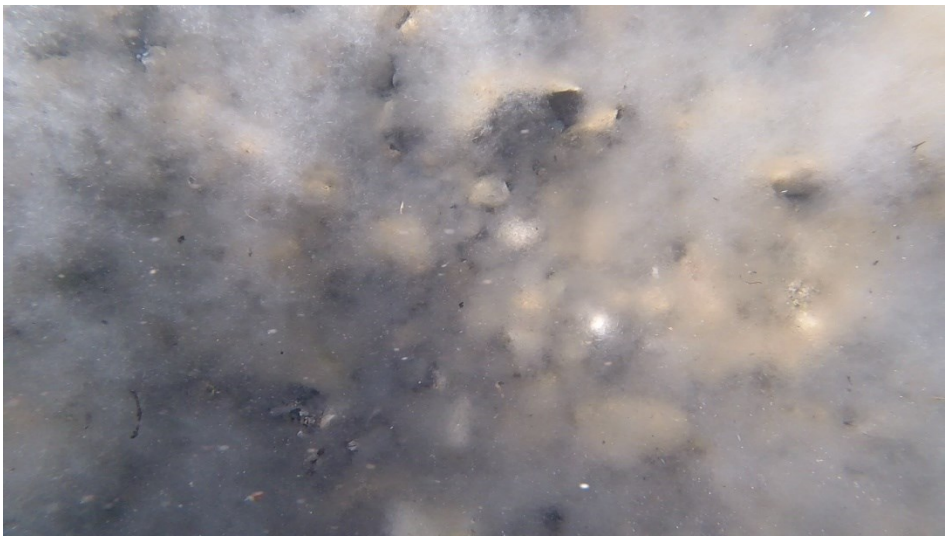

Figure 2-1. Digital image showing anchor ice forming around gravel in the Kananaskis River, December 8, 2016 (field of view is ~2m).

Figure 2-2. Digital image showing a rock (~5 cm diameter) resting on top of an anchor ice formation in the Kananaskis River, December 8, 2016.

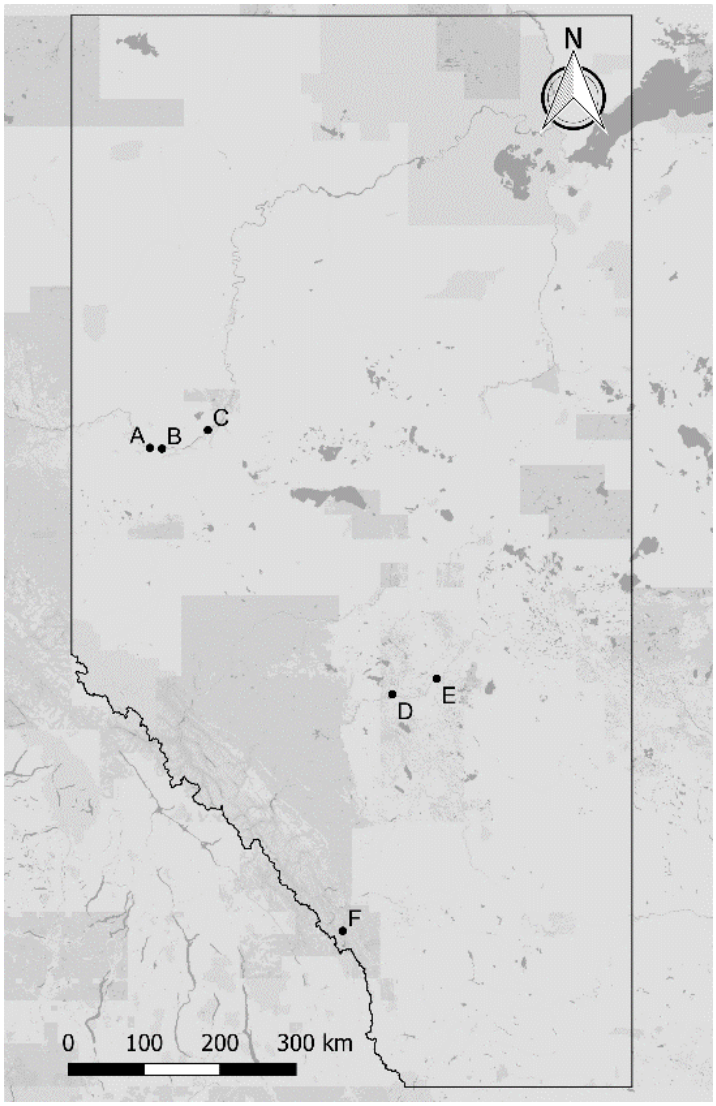

Figure 2-3. Map of the province of Alberta showing the anchor ice sampling locations. Peace River sites (A) the Dunvegan boat launch, (B) Fairview Intake and (C) Shaftesbury Ferry crossing; North Saskatchewan River sites, (D) Genesee boat launch and (E) City of Edmonton sites (Emily Murphy Park and Quesnell); Kananaskis River site (F) Fortress Mountain Resort bridge.

Figure 2-4. Digital image of a drained anchor ice sample collected using an ice scoop, November 28, 2016. The width of the scoop as indicated by the arrow is ~18 cm.

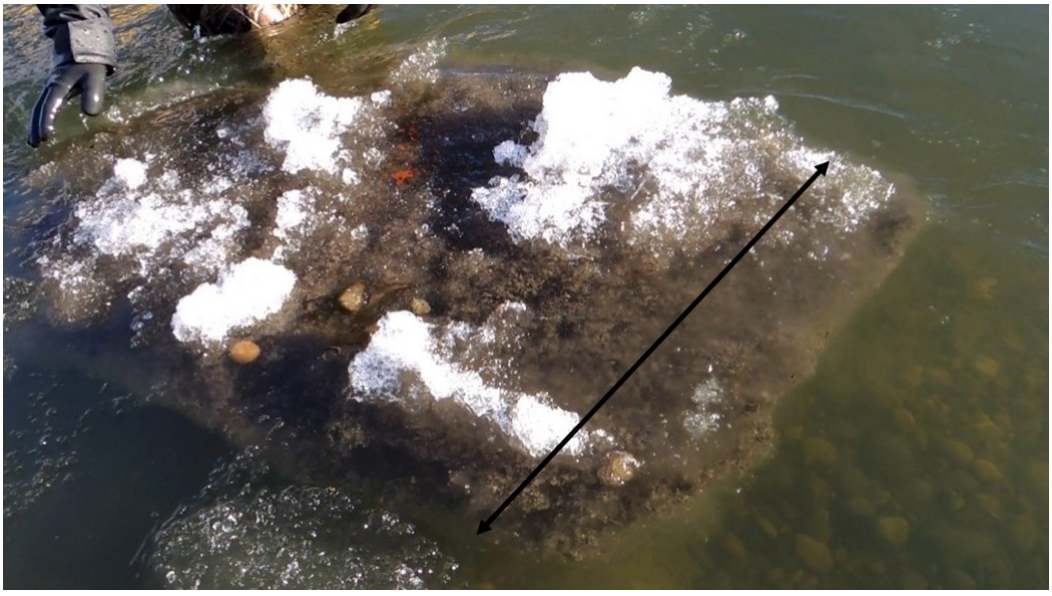

Figure 2-5. Digital image of an anchor ice pan rafting sediments on the North Saskatchewan River at Genesee, December 3, 2016. The width of the anchor ice pan as indicated by the arrow is ~1 m.

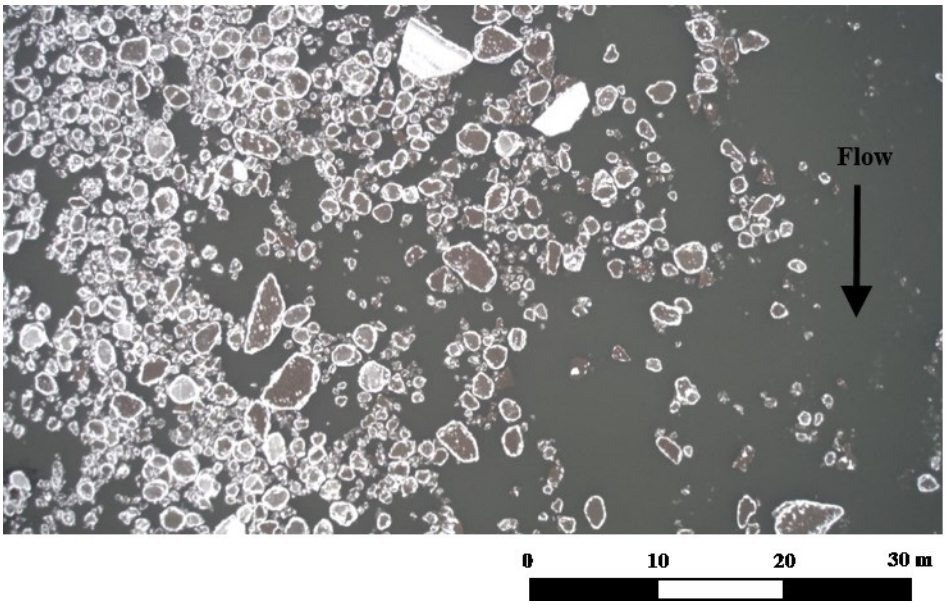

Figure 2-6. Digital image taken with an unmanned aerial vehicle of an anchor ice release event on the Peace River at the Dunvegan boat launch, January 14, 2017.

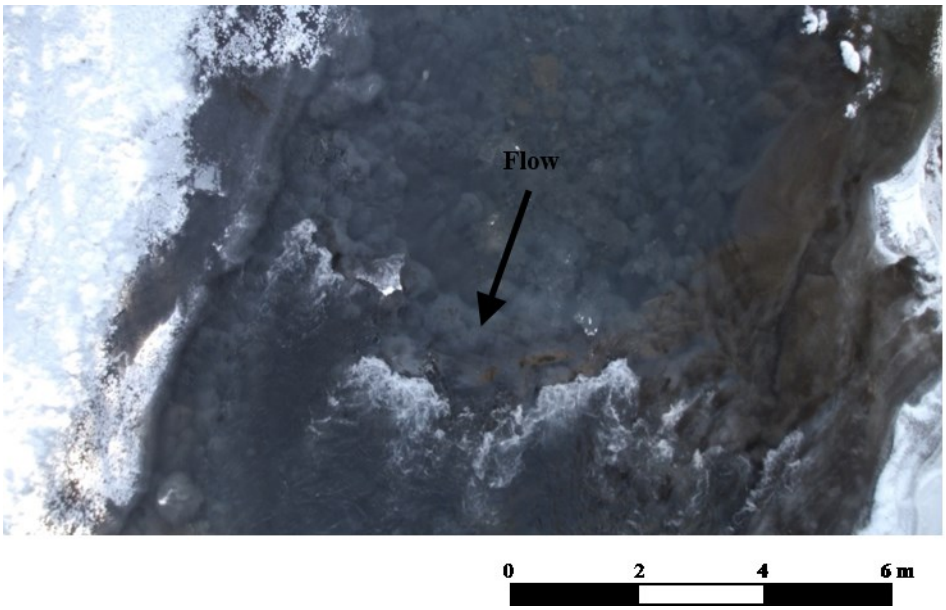

Figure 2-7. Digital image taken with an unmanned aerial vehicle showing a large anchor ice weir on the Kananaskis River at Fortress, December 8, 2016 (aerial image obtained under permit from AB Parks).

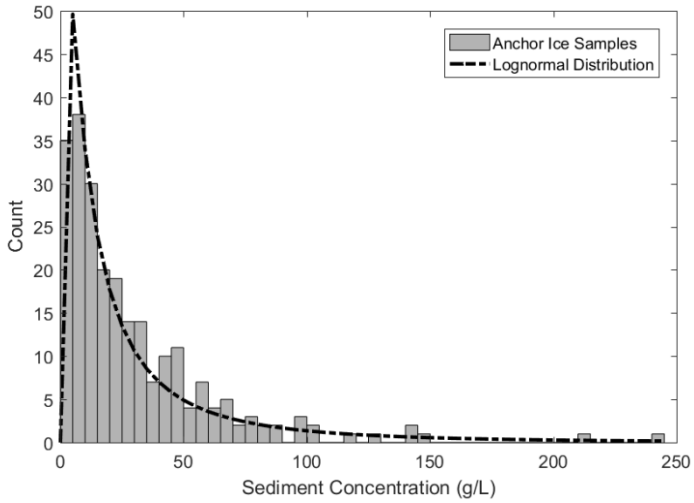

Figure 2-8. Histogram of measured sediment concentration from anchor ice samples, with a bin size of 5 g/L (N = 239).

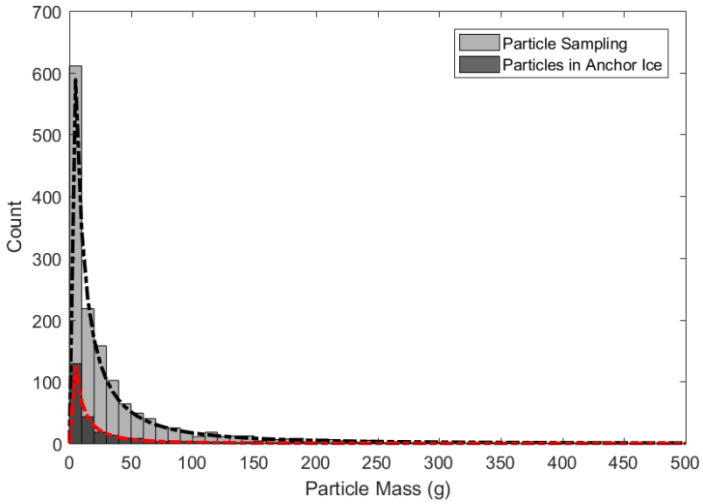

Figure 2-9. Histograms of the mass of particles found through particle sampling and contained in anchor ice samples from the winter of 2016 to 2017. Bin size is 10 g. Note there were 18 particles with masses greater than 500 g that are not shown. The black and red dashed lines represent lognormal distributions for both data sets computed using the corresponding mean and standard deviation.

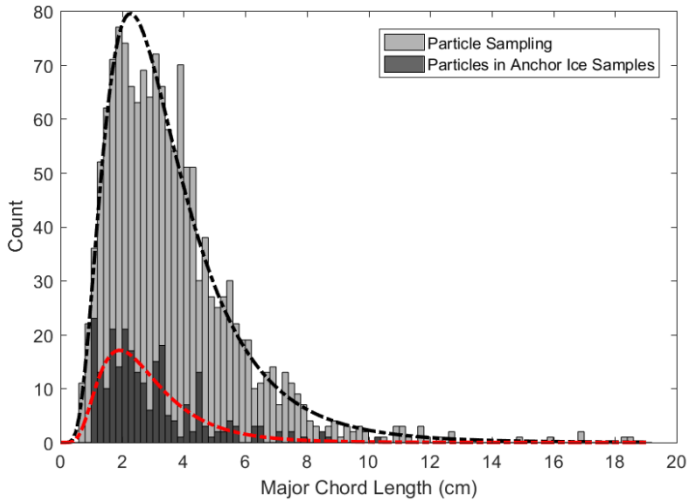

Figure 2-10. Histograms of the major chord length of particles found through particle sampling and contained in anchor ice samples from the winter of 2016 to 2017. Bin size is 0.2 cm. The black and red dashed lines represent the lognormal distributions data sets computed using the corresponding mean and standard deviation.

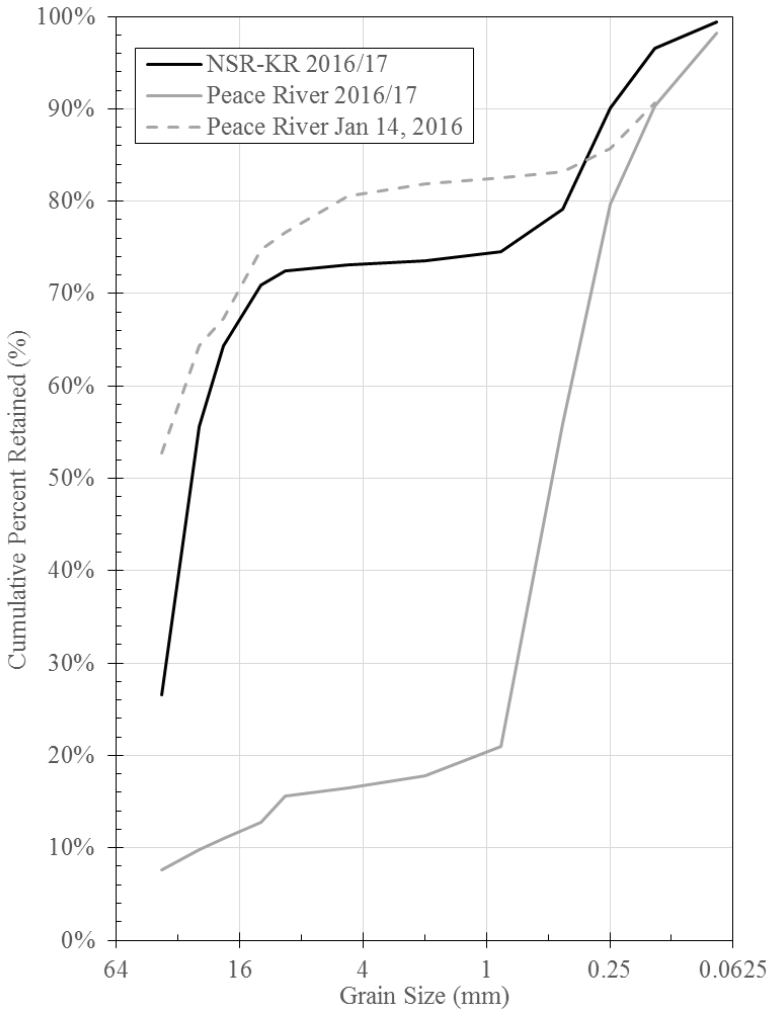

Figure 2-11. Cumulative percent retained on the sieve plot of sediment found in anchor ice samples. Note that the x-axis scale is base-2 log scale

Tables

Table 2-1. Description of anchor ice sampling sites

River	Site	Coordinates
North Saskatchewan River	Emily Murphy Park	53°31’56”N 113°31’53”W
	Quesnell	53°30’20”N 113°33’60”W
	Genesee	53°22’38”N 114°16’51”W
Peace River	Fairview Intake	55°54’34”N 118°23’34”W
	Dunvegan	55°55’8”N 118°36’18”W
	Shaftesbury	56°5’43”N 117°34’18”W
Kananaskis River	Fortress	50°47’14”N 115°9’56”W

Table 2-2. Summary of the data from the analysis of anchor ice samples including the range of total fixed solids (TFS) and total volatile solids (TVS).

River	Site	Date	Number of Samples Collected	TFS Range (g/L)	TVS Range (g/L)
North Saskatchewan River	Emily Murphy Park	19-Nov-15	4	1.8 - 21.0	0.08 - 0.23
		26-Nov-16	11	0.3 - 68.2	0.00 - 0.20
		27-Nov-16	9	0.7 - 242.0	0.05 - 0.54
		28-Nov-16	11	0.9 - 64.8	0.00 - 5.03
	Quesnell	24-Nov-16	11	0.5 - 98.3	0.00 - 0.59
		25-Nov-16	7	0.2 - 81.8	0.02 - 4.18
	Genesee	3-Dec-16	30	5.4 - 212.6	0.00 - 0.42
Peace River	Fairview Intake	14-Jan-16	3	19.0 - 26.1	-
		21-Feb-16	14	0.6 - 43.4	0.01 - 0.57
	Dunvegan to Fairview	21-Jan-16	3	8.1 - 129.5	0.08 - 1.43
	Dunvegan	23-Jan-16	3	5.8 - 32.6	0.00 - 0.57
		23-Feb-16	19	2.7 - 86.2	0.06 - 0.93
		14-Jan-17	24	1.1 - 142.5	0.00 - 0.64
		15-Jan-17	25	3.2 - 98.0	0.08 - 1.21
	Shaftesbury	15-Jan-17	30	5.4 - 147.2	0.10 - 1.91
Kananaskis River	Fortress	7-Dec-16	25	0.3 - 140.1	0.05 - 1.79
		8-Dec-16	10	8.4 - 100.3	0.02 - 4.18

Table 2-3. Mean sediment concentrations contained in anchor ice by river and winter season.

River	Winter Season	Mean Sediment Concentration (g/L) (± standard deviation)
North Saskatchewan River	2015-2016	11.9 ± 7.8
Peace River	2015-2016	26.3 ± 26.1
North Saskatchewan and Peace Rivers	2015-2016	25.0 ± 25.3
North Saskatchewan River	2016-2017	29.0 ± 42.1
Kananaskis River	2016-2017	37.7 ± 34.0
Peace River	2016-2017	29.4 ± 26.7
North Saskatchewan, Peace, and Kananaskis Rivers	2016-2017	30.7 ± 35.0
TOTAL	2015-2017	29.6 ± 33.4

Table 2-4. Mass retained for sieved sediment contained in anchor ice samples.

Sieve Number	Opening Size (mm)	Mass Retained (%)		
		North Saskatchewan - Kananaskis River 2016-2017	Peace River 2016-2017	Peace River Jan. 14, 2016
1 1/2"	38.1	26.5%	7.6%	52.8%
1"	25	29.1%	2.1%	11.5%
3/4"	19.1	8.8%	1.3%	3.1%
1/2"	12.5	6.5%	1.8%	7.4%
3/8"	9.51	1.5%	2.9%	1.9%
No. 4	4.75	0.7%	0.8%	4.0%
No. 10	2	0.4%	1.3%	1.2%
No. 20	0.85	1.0%	3.3%	0.7%
No. 40	0.425	4.6%	34.9%	0.7%
No. 60	0.25	10.9%	23.8%	2.5%
No. 100	0.15	6.5%	10.5%	4.9%
Pan	0.075	2.8%	7.9%	9.3%

References

Church, M., 2015. The regulation of Peace River: a case study for river management. John Wiley & Sons, Ltd., Chichester, West Sussex, UK.

Daly, S., 1994. Report on frazil ice.

Dayton, P.K., Robilliard, G., Devries, A.L., 1969. Anchor ice formation in McMurdo Sound, Antarctica. American Association for the Advancement of Science, Washington, D.C.

Doering, J., Bekeris, L., Morris, M., Dow, K., Girling, W., 2001. Laboratory Study of anchor ice growth. J. Cold Reg. Eng. 15, 60–66.

Emmer, S., Nafziger, J., McFarlane, V., Loewen, M., Hicks, F., 2013. Winter Ice Processes of the Kananaskis River, Alberta, in: Proceedings of the 17th Workshop on River Ice. Committee on River Ice Processes and the Environment, Edmonton, AB.

Girling, W., Groeneveld, J., 1999. Anchor ice formation below Limestone Generating Station. Manitoba Hydro, Winnipeg, MN.

Gosink, J., Osterkamp, T., 1986. Frazil ice nucleation by ejecta from supercooled water, in: Proceedings of the 8th IAHR Symposium on Ice. Iowa City, Iowa, pp. 249–263.

Hirayama, K., Terada, K., Sato, M., Hirayama, K., Sasamoto, M., Yamazaki, M., 1997. Field measurements of anchor and frazil ice, in: Proceedings of the 9th Workshop on River Ice. Fredericton, NB.

Jasek, M., Shen, H.T., Pan, J., Paslawski, K., 2015. Anchor ice waves and their impact on winter ice cover stability, in: Proceedings of the 18th Workshop on the Hydraulics of Ice Covered Rivers. Quebec City, QC.

Kalke, H., Loewen, M., McFarlane, V., Jasek, M., 2015. Observations of anchor ice formation and rafting of sediments, in: Proceedings of the 18th Workshop on the Hydraulics of Ice Covered Rivers. Quebec City, QC.

Kalke, H., Schneck, C., McFarlane, V., Loewen, M., Jasek, M., 2016. Ice rafting of sediment by anchor ice releases, in: Proceedings of the 22nd IAHR International Symposium on Ice. Ann Arbor, Michigan.

Kellerhals, R., Neill, C.R., Bray, D.I., 1972. Hydraulic and Geomorphic Characteristics of Rivers in Alberta. Edmonton, AB.

Kempema, E., Ettema, R., 2011. Anchor ice rafting: observations from the Laramie River. River Res. Appl. 27, 1126–1135.

Kempema, E., Ettema, R., McGee, B., 2008. Insights from anchor ice formation in the Laramie River, Wyoming, in: Proceedings of the 19th International Symposium on Ice. Vancouver, BC.

Kempema, E.W., Reimnitz, E., Barnes, P.W., 2001. Anchor-ice formation and ice rafting in southwestern Lake Michigan, U.S.A. J. Sediment. Res. 71, 346–354. doi:10.1306/2DC40948-0E47-11D7-8643000102C1865D

Kempema, E.W., Reimnitz, E., Clayton, J.R., Payne, J.R., 1993. Interactions of frazil and anchor ice with sedimentary particles in a flume. Cold Reg. Sci. Technol. 21, 137–149.

Kempema, E.W., Reimnitz, E., Hunter, R.E., 1986. Flume studies and field observations of the interaction of frazil ice and anchor ice with sediment. U.S. Geological Survey, Menlo Park, California.

Kerr, D.J., Shen, H.T., Daly, S.F., 2002. Evolution and hydraulic resistance of anchor ice on gravel bed. Cold Reg. Sci. Technol. 35, 101–114.

Kerr, D.J., Shen, H.T., Daly, S.F., 1997. Anchor ice formation and growth on gravel channel bed, in: Proceedings of the 9th Workshop on River Ice. Fredericton, NB.

Nafziger, J., She, Y., Hicks, F., Cunjak, R.A., 2017. Anchor ice formation and release in small regulated and unregulated streams. Cold Reg. Sci. Technol. 141, 66–77. doi:10.1016/j.coldregions.2017.05.008

Osterkamp, T.E., 1978. Frazil Ice Formation: A Review. J. Hydraul. Div.

Qu, Y.X., Doering, J., 2007. Laboratory study of anchor ice evolution around rocks and on gravel beds. Can. J. Civ. Eng. 34, 46–55.

Smedsrud, L., 2001. Frazil-ice entrainment of sediment : large-tank laboratory experiments. J. Glaciol. 47, 461–471.

Stickler, M., Alfredsen, K., 2009. Anchor ice formation in streams: a field study. Hydrol. Process. 23, 2307–2315.

Terada, K., Hirayama, K., Sasamoto, M., 1998. Field Measurements of Anchor and Frazil Ice, in: Proceedings of the 14th International Symposium on Ice. International Association for Hydro-Environment Envineering and Research, Potsdam, NY.

Tremblay, P., Leconte, R., Jay Lacey, R.W., Bergeron, N., 2014. Multi-day anchor ice cycles and bedload transport in a gravel-bed stream. J. Hydrol. 519, 364–375.

Tsang, G., 1982. Frazil and anchor ice: a monograph. NRC Subcommittee on Hydraulics of Ice Covered Rivers, Ottawa, ON.

Wigle, T.E., 1970. Investigations into frazil, bottom ice and surface ice formation in the Niagara River, in: Proceedings of the 1st International Symposium on Ice. International Association for Hydro-Environment Envineering and Research, Reykjavik, Iceland.

Yamazaki, M., Hirayama, K., Sakai, S., Sasamoto, M., Kiyohara, M., Takiguchi, H., 1996. Formation of frazil and anchor ice, in: Proceedings of the 13th International Symposium on Ice. International Association for Hydro-Environment Envineering and Research, Beijing, China.

Chapter 3 Support Vector Machine Learning Applied to Digital Images of River Ice Conditions[2]

3.1 Introduction and Background

Surface ice cover development is a complex process that occurs in northern rivers exposed to sustained freezing air temperatures. The initial stage of river ice formation occurs when the water column is supercooled and frazil is generated. Frazil ice crystals are inherently adhesive in nature and begin to flocculate together, forming frazil flocs that rise to the water surface when they become sufficiently buoyant. In the early stages of freeze-up, surface slush appears on the water surface. As freeze-up progresses and the surface slush is exposed to freezing air temperatures, frazil ice pans are observed on the water surface. Mature frazil ice pans are observed to be circular with upturned edges from colliding with other frazil ice pans in the flow. Frazil pans often freeze together in the late stages of freeze-up, forming large frazil ice rafts. Once the surface concentration is high enough, a juxtaposed ice cover can begin to form at a point of constriction where frazil ice pans bridge and become immobile.

Anchor ice can also be observed along with frazil ice in the flow and may at times comprise the entirety of the surface ice concentration. At freeze-up, anchor ice can be released from the bed of a river through thermal (see Tsang, 1982) or mechanical means (see Kerr et al., 2002). Released anchor ice has been observed to transport bed material downstream, and is often observed to appear as "dirty" ice pans in the flow (e.g. Kalke et al., 2016, 2015). During an anchor ice release event, there are significantly more anchor ice pans on the water surface since frazil generation has stopped. During some anchor ice release events on the Peace River virtually all the observed pans were anchor ice (Kalke et al., 2017).

[2] This chapter has been submitted for publication to Cold Regions Science and Technology as Kalke, H. and Loewen, M. 2017. Support vector machine learning applied to digital images of river ice conditions.

Surface ice concentration, both frazil and anchor ice, is an important parameter to help in understanding freeze-up processes leading to the formation of a solid ice cover. Total surface ice concentration is defined as the percentage of the water surface that is covered by frazil and anchor ice pans. The total surface ice concentration can be computed by capturing digital images of the river during freeze-up and processing the images using an image processing algorithm, such as thresholding or machine learning, to separate the surface ice from the water. Computing the total surface ice concentration can also aid in the validation of river ice dynamic models that predict surface ice concentrations leading to a solid ice cover formation (e.g. CRISSP2D (Shen et al., 2000, 1993), RIVICE (Lindenschmidt, 2017), and ICESIMAT (Zare et al., 2015)). Computing the concentration of anchor ice in the flow is also of interest, since it can assist with estimating the amount of sediment transported through this process. Currently, the amount of sediment transported by anchor ice over a winter season and its contribution to the annual sediment budget is unknown. Developing an algorithm to compute the amount of anchor ice in the flow at a given time will allow for better estimates of sediment transport by anchor ice to be made. Total surface ice concentration has been computed using fairly standard automated image processing techniques (e.g. Ansari et al., 2017); however, computing the concentration of anchor ice, that is distinguishing between frazil and anchor ice pans, is a more challenging problem.

In this study, binary images differentiating between total surface ice (i.e. the sum of frazil and anchor ice pans) and water in a digital image are created through traditional thresholding techniques (automated and manual thresholding) and a learning model, the support vector machine (SVM). The SVM is a popular "off the shelf" model for machine learning. This type of model is a two-group classifier that can be trained to distinguish between two unique types of information appearing in images such as ice and water or frazil and anchor ice. SVMs are advantageous over traditional linear separators (e.g. thresholding) since they are able to embed the

training data into higher-dimensional space where finding a separator for two groups of data is more accurate (Russell and Norvig, 2010). Three site-specific SVMs were trained to distinguish total surface ice from the water in a digital image, and one SVM was trained to further separate the total surface ice into the frazil and anchor ice components on the Peace River. The binary prediction results using thresholding techniques and the SVMs are discussed and compared. A detailed description of the SVM model training and implementation is also presented. This study builds on preliminary work presented in Kalke and Loewen (2017).

3.2 Literature Review – Image Processing

3.2.1 Thresholding

Thresholding is a basic image processing method to separate objects in the foreground from the background of the image based on grayscale or colour pixel values. In this method a threshold is selected and pixels are replaced with a white or black pixel if the value is above or below the threshold, respectively. This produces a binary image that has only two possible values, 1 or 0, for each individual pixel. A simple widely used technique is to set a constant threshold and apply this threshold to multiple images. This type of thresholding is subjective, applicable only to images that have very similar histograms (i.e. no changes in colour or brightness), and generally not practical as it cannot adapt to changes over time in the image histogram (Russ, 2007).

Automated thresholding techniques are consistent between users and are able to adapt to changes in the histogram. These techniques can be categorized into two major types, global and local thresholding (Ansari et al., 2017). Global thresholding separates foreground objects in an image from the background using one threshold value applied to all the pixels in an image but a new threshold value is computed for each image. This technique can also be performed manually by the user setting a threshold value for each image; however, this is time consuming and can produce

differing results between users (Russ, 2007). Therefore, global threshold selection through an automated technique is preferred and Otsu's Method (Otsu, 1979) is a popular method. However, global thresholding often fails if the foreground objects of interest have significantly different gray values, even if the background is uniform (Jähne, 1997). Significant spatial variations within the image can also cause global threshold methods to fail since only one threshold value is used in each image (Ansari et al., 2017). A method designed to account for spatial variations is local thresholding. This is an automated method that computes a local threshold value for each individual pixel based on first-order statistics (i.e. mean or median) of the neighbourhood pixel intensities (Ansari et al., 2017).

3.2.2 SVM Learning

Machine learning is a type of artificial intelligence that allows computers to learn from experience without the need for detailed programming (Samuel, 1959). A machine is trained with a given set of data to predict information or properties about a new set of data (Segaran, 2007). These types of learning models can range from completely transparent, where it is easy to understand why the decisions were made, to a complete "black box" model, where it is difficult to reproduce the reasoning behind the results (Segaran, 2007). Machine learning algorithms can be reduced to two categories of learning: supervised or unsupervised. For supervised learning, the machine is given the training data examples along with the desired binary solutions for each example (Segaran, 2007). For unsupervised learning the machine is not given the desired solutions, but instead infers the binary solutions by clustering the data into two groups (Segaran, 2007).

The SVM is a learning algorithm that can be used for two-group classification (Cortes and Vapnik 1995). SVMs are the most popular "off the shelf" learning model and can be applied using a variety of programming languages (Russell and Norvig, 2010). SVMs are advantageous over traditional linear separators (e.g. thresholding) since they can embed the training data into higher-dimensional space

where a separating hyperplane may be found (Russell and Norvig, 2010). The optimum hyperplane is constructed by finding the maximum margin between the two groups of data (Cortes and Vapnik, 1995). This is achieved by only considering the data points closest to this separator; these points are referred to as the "support vectors" (Cortes and Vapnik, 1995). These higher-dimensional hyperplane separators are non-linear in the original space, which greatly expands the prediction capabilities over linear separators (Russell and Norvig, 2010). SVMs have been used for object recognition in digital images such as facial recognition (e.g. Osuna et al., 1997) and handwriting recognition (e.g. Choisy and Belaid, 2001).

3.2.3 SLIC Superpixels

Superpixels are pixels that are grouped together into meaningful regions by a superpixel algorithm (Achanta et al., 2011). These superpixels are able to reduce the complexity of an image for subsequent image processing by capturing the redundancy within an image (Achanta et al., 2010). The redundant areas become captured within one superpixel, and then subsequent image processing tasks only compute information with regard to one superpixel rather than each of the pixels contained within the superpixel. This reduces the computational complexity by reducing the millions of pixels contained in an image with thousands of superpixels. Applying a superpixel algorithm to a digital image during pre-processing is a popular strategy since it is easier for machine learning algorithms to deal with hundreds or thousands of superpixels rather than millions of raw pixels (Russell and Norvig, 2010). The Simple Linear Iterative Clustering (SLIC) algorithm is a preferred method for forming superpixels because of its overall performance (i.e. excellent boundary adherence, memory usage, and computation speed) when compared to other superpixel algorithms (Achanta et al., 2011). SLIC Superpixels are clusters of pixels that are formed based on pixel LAB colour values and spatial x, y coordinates using the SLIC algorithm. The LAB colour space represents the lightness, its position between red and green, and its position between blue and yellow, respectively. This technique is effective for a variety of applications,

including image segmentation and computer vision. Superpixels are relatively easy to implement in an image processing algorithm since the user only needs to specify the desired number of superpixel clusters.

3.3 Study Sites

Digital images of surface ice conditions were captured during the winters of 2015-2016 and 2016-2017 on two Alberta Rivers, the North Saskatchewan River and the Peace River. Figure 3-1 and Figure 3-2 show the study locations on the North Saskatchewan and Peace River, respectively. The North Saskatchewan River flows northeast from the Bighorn and Brazeau Dams in southwest Alberta through the City of Edmonton. The approximate drainage area of the North Saskatchewan River is 125,000 km^2 (Kellerhals et al., 1972). The average winter flow in the City of Edmonton, between October and March, is 126 m^3/s based on average daily flow data from 1972-2012 at the Water Survey of Canada gauge 05DF001. Kellerhals et al. (1972) report an average depth of 1.4 m for a long-term mean discharge of 218 m3/s. The freeze-up on the North Saskatchewan River begins mid to late November and a solid ice cover typically forms within ~1 to 2 weeks and persists until break-up in the spring.

The Peace River flows east from the W.A.C. Bennett and Peace Canyon Dam in British Columbia through the Town of Peace River in Alberta. The total drainage area of the Peace River is roughly 293,000 km^2 in both Alberta and northern British Columbia (Church, 2015). This study focuses on ice conditions at the Dunvegan Bridge boat launch and the Shaftesbury Ferry Crossing, which are 296 km and 370 km downstream of the W.A.C. Bennett Dam, respectively. Mean annual flow at the Dunvegan Bridge, between October and March, is approximately 1524 m^3/s, based on daily average flow data at the Water Survey of Canada gauge 07HA003 from 1981 (post-construction of the Peace Canyon Generating Station) to 2016. Using the hydraulic geometry equations for the Peace River at Dunvegan provided by Church (2015), the average depth, width, and velocity for an average winter

discharge of 1524 m^3/s are 3.2 m, 369 m, and 1.31 m/s, respectively. On the Peace River, regulation by the W.A.C. Bennett and Peace Canyon Dams causes a significant portion of the downstream reach to remain open throughout the entirety of the winter season. The leading edge of the ice cover on average, between 1973 to 2007, has developed to ~250 km downstream of the W.A.C. Bennett dam before retreating during the spring thaw (Alberta Environment and Parks, 2017). As a consequence of this open water, frazil and anchor ice generation can often be observed throughout much of the winter season at the two study sites.

3.4 Methodology

3.4.1 Image Acquisition and Instrumentation

Digital images of surface ice conditions on the North Saskatchewan River in the City of Edmonton were captured with Reconyx PC800 Hyperfire Professional game cameras. In Figure 3-3a, a typical digital image taken with a game camera on the North Saskatchewan River is presented. In Figure 3-3b, a typical digital image taken with the UAV on the Peace River is presented. The game cameras were mounted to the hand railing of two pedestrian bridges in the City of Edmonton between November 15 and December 18, 2016: (1) Dudley B. Menzies Bridge and (2) Fort Edmonton Footbridge. In Figure 3-4 an image showing how the game cameras were mounted and secured to the side railing of the Fort Edmonton Footbridge using PVC pipe. This allowed the cameras to be oriented parallel with the water surface so no image rectification was required. The game camera mounts on the Dudley B. Menzies Bridge were designed similarly. A weather station deployed at the Mayfair Golf and Country Club (53°33’62”N 113°32’85”E) near the University of Alberta in Edmonton provided air temperature measurements throughout the 2016-2017 winter season.

Game camera image resolution was 3.1 megapixels and images were captured at a one minute frequency between daylight hours (9am to 4pm). Three cameras were

mounted to each bridge near the left bank, mid-channel, and right bank. Cameras mounted on both pedestrian bridges in the City of Edmonton were approximately 14.3 m above the water surface during freeze-up, which resulted in a field of view of 11.1 m. The left bank camera on the Fort Edmonton Footbridge was lost due to vandalism along with all its data. Digital images acquired from the bridge-mounted game cameras were used to obtain a time-series of the surface ice concentration throughout freeze-up in the City of Edmonton. Surface ice concentration was computed from each image and the average surface ice concentration in the channel was computed by averaging the values from two or three cameras.

Digital images of surface ice were also captured with a Blade Chroma UAV equipped with a CGO3 4K camera on the North Saskatchewan River at the Genesee boat launch and on the Peace River at the Dunvegan Bridge boat launch and Shaftesbury Ferry crossing. A typical UAV image acquired during a flight at the Dunvegan Bridge is displayed in Figure 3-3b. UAV flights occurred on the Peace River January 21-23, 2016 and January 14-15, 2017. UAV flights on the North Saskatchewan River at the Genesee boat launch occurred on December 1 and 3, 2016. The UAV was flown perpendicular to the flow with its digital camera pointed directly downwards at the water surface to capture high-resolution continuous video of the ice conditions. Digital images were extracted from the continuous video at 5 second intervals in MATLAB with a resolution of 8.3 megapixels.

Digital images acquired with the UAV were used to compute a spatial distribution of concentration across the width of the channel for the North Saskatchewan River at Genesee on December 3, 2016 and on the Peace River at the Dunvegan boat launch on January 14, 2017. On the North Saskatchewan River at Genesee, the UAV was flown directly above the center of the channel and could capture the entire cross-section within the image. This allowed for the UAV to be fixed at one position for ~9.5 minutes while continuously video recording surface ice conditions. Digital images were then extracted from the continuous video at five second intervals, and a complete instantaneous spatial distribution could be

computed from each extracted digital image and a time-averaged spatial distribution over the entire 9.5-minute period. On the Peace River at the Dunvegan Bridge, the UAV could not be flown high enough (i.e. maximum permissible height is 90 m, which equates to roughly 180 m of river width captured in the image) to permit the entire cross-section to be captured in a single image. Therefore, the UAV was flown across the channel at an approximately constant speed while continuously recording video. This sequence of images was then used to compute a spatial distribution of surface ice concentration over the entire width of the river. Images were scaled by beginning the continuous video recording while hovering at the flight elevation over a 2-meter long painted board placed near the water surface prior to each UAV flight.

The UAV altitude was unchanged for the duration of the flight and the speed remained approximately constant, so distance from the bank could be estimated for each image. Digital images used to compute the two spatial distributions were first segmented into smaller sub-images 10-meter wide in the transverse direction. The surface concentration in each sub-image was computed and the location of this measurement was assumed to be the center of this sub-image from the left bank. The UAV was assumed to travel at a constant speed of 2.4 m/s, this was estimated from a total flight distance of ~200 meters measured in Google Earth and a travel time of ~85 seconds from the continuous video. The UAV distance from the left bank was adjusted for each subsequent image as the drone moved at a constant speed.

3.4.2 Image Processing

3.4.2.1 Thresholding

The following four thresholding methods were tested in this study: (1) applying a single grayscale threshold to multiple images (constant thresholding), (2) manually applying a new threshold to the grayscale image for each individual image (manual

global thresholding), (3) automated local thresholding with *graythresh* in MATLAB that uses Otsu's Method and, (4) automated global thresholding with *adaptthresh* in MATLAB.

3.4.2.2 Support Vector Machine Training

In this study, a supervised method of training was employed for the two-group classifier SVMs. A learning model such as the support vector machine is trained to classify data by example; this means that training examples need to be provided during training with the desired solution or "response". The model chosen in this study is a two-group classifier, although an SVM can be trained for multiple classes and for regression problems. Training the SVM in MATLAB involves inputting a matrix of example data (training matrix) and the corresponding response vector (binary training vector) into the *fitcsvm* function to obtain a trained model. Each row of the training matrix is one training example and each column in the training matrix is a feature associated with the example (i.e. pixel values, statistical properties, texture information, etc). Each row of the binary training vector is the binary value associated with the corresponding row or "example" in the training matrix. A trained *ClassificationSVM* model object is then outputted and can be used to predict new binary images.

Three models were trained to predict total surface ice concentration at three different sites: (1) Peace River with digital images acquired with the UAV (PR-UAV), (2) North Saskatchewan River with digital images acquired with the game cameras on the two bridges in the City of Edmonton (NSR-GC), and (3) North Saskatchewan River at Genesee with digital images acquired with the UAV (NSR-UAV). The number of training images used was selected to ensure that all the different ice types and lighting conditions were trained into each model. The PR-UAV, NSR-UAV, and NSR-GC models to predict total surface ice concentration were trained with 161, 31, and 33 training images, respectively. The PR-UAV model had considerably more training images since the ice and lighting conditions

varied significantly more during these deployments. Training images provided to the model consisted of raw training images (Figure 3-5a), and manually created corresponding binary images (Figure 3-5b), referred to here as "binary training images", where the ice is separated from the water. UAV digital images were large (3840 x 2160 pixels) and were cropped into smaller images (1280 x 1080 pixels) to make the manually creating binary images more manageable. Game camera images were 2048 x 1536 pixels and were only cropped to remove the information printed along the top by the game camera software, see Figure 3-3. The digital images acquired in this study contained either surface ice or water. The binary training images are created by colour thresholding the raw training images by trial and error using MATLAB's "Color Thresholding" built-in application. This application allows thresholds to be modified directly while the corresponding binary image is displayed. The resulting binary images then needed to be corrected manually using the photo editing software GIMP (GNU Image Manipulation Program) 2.0 since thresholding was not capable of correctly identifying all the surface ice.

The "examples" or each row of the training matrix consisted of features associated with the superpixels in each raw digital image. The statistics of the pixels contained in each superpixel are used as the examples in the training matrix. The features (i.e. columns in the training matrix) for each superpixel consisted of 81 computed statistics of the pixels contained within each superpixel. A single row with 81 features in the training matrix is created by computing 33 statistical features within a superpixel, and 48 statistical features in a 100x100 pixel grid around the centre of the superpixel. The neighbourhood information was arbitrarily selected to improve model results; it was found to slightly improve the model performance so it was included in the final model. There were 11 features extracted from pixels contained within each superpixel, these included: mean, standard deviation, max, min, median, root-mean-square, skewness, kurtosis, variance, and normalized x, y spatial values. This was done for three colour channels (hue, saturation, and value (HSV)), so 33 features were extracted in total from the superpixel. The remaining 48 features were obtained from the neighbouring pixel values in each of the three

colour channels. A grid of 100x100 pixels around each superpixel was created and then divided into four 50x50 subareas. The max, min, mean, and standard deviation of the pixels contained in each of the four grids was computed. This was done for each of the three colour channels (HSV), which made up the remaining 48 features (i.e. each of the four grids had four computed statistical features in each of the three colour channels). The binary value (ice or water) associated with the 81 statistical features was computed as the mode of the binary pixel values in the binary training image. Each row of the training matrix consists of the 81 statistical features for each superpixel within each of the training images. The binary training vector contains the corresponding binary value for each row of the training matrix.

The procedure for creating the training matrix and binary training vector was virtually the same for all SVM models; the exception being that in the binary training matrix for the anchor ice delineation model (described in detail in the next section) 1's and 2's corresponded to frazil and anchor ice and pixels that corresponded to water within the image were ignored. First, the raw training images were smoothed using the function *imgaussfilt3* in MATLAB which allowed the superpixel algorithm to find the boundaries more easily. Second, the superpixel algorithm was applied to the smoothed digital image, which outputs a matrix identifying which pixels are contained within each superpixel. Each of the training images in this study were segmented into 10,000 superpixels. Third, the raw digital images were then converted from the RGB to HSV (hue, saturation, and value) colour space with the function *rgb2hsv* function in MATLAB. Fourth, the 81 statistical features for each superpixel in all the training image and the corresponding binary value from the binary training image were computed and inserted into a row of the training matrix and binary training vector, respectively. Fifth, once the training matrix and binary training vector was constructed the SVM was trained using the *fitcsvm* function. The *fitcsvm* function outputs a trained *ClassificationSVM* model object in MATLAB that could then be used to predict binary images from raw digital images.

This model was then used with the *predict* function in MATLAB to predict new binary images for any digital image. The *predict* function requires an input matrix, constructed using the same steps used for constructing the training matrix, and a *ClassificationSVM* model object to predict a new binary image. The full-size UAV digital images (3840 x 2160 pixels) are six times larger than the cropped images (1280 x 1080 pixels) used for training, therefore when processing these full-size UAV digital images, 60,000 superpixels are used. The game camera images were similar in size to the game camera images used for training, so 10,000 superpixels are used when processing these images. The output from the *predict* function is a binary vector indicating either ice or water for each superpixel contained in the digital image. The final step is then to construct a binary image from the predicted vector of binary values. This is performed by creating a new blank image in MATLAB with the same dimensions as the digital image; this can be done by creating a matrix of zeros with the same dimension as the raw digital image. Within this blank image each of the predicted binary values (i.e. 0 or 1) are inserted into the location of the pixels contained within the superpixel from the original digital image.

It was observed that predicted binary labels for superpixels were occasionally mislabeled. These mislabeled superpixels appeared as holes (black pixel regions) within the surface ice or as scattered white pixel regions surrounded by water. Morphological operations using the *bwareaopen* function were performed to fill in these holes within ice covers and to remove these erroneous small white pixel regions. It was determined by trial and error that the most accurate binary images were produced when holes with at least 5000 pixels were filled and white pixel regions smaller than 250 pixels were blacked out for images taken with the UAV. The images taken with the game cameras were observed to improve by filling in larger holes than the UAV processed images (i.e. holes with at least 10,000 pixels were filled for game camera images). This is a result of the height at which each instrument is deployed and the relative scale of the digital images. White pixel

regions smaller than 250 pixels were also blacked out in the binary images created from the game camera images.

3.4.2.3 Support Vector Machine for Anchor Ice Delineation

The fourth SVM was trained to separate the total surface ice predicted by the PR-UAV model into the frazil and anchor ice components. An example of a raw UAV training image is shown in Figure 3-6a along with the corresponding labelled training image in Figure 3-6b. The total surface ice in Figure 3-5b was labelled as either frazil or anchor ice, which produced the labelled training image shown in Figure 3-6b. Labelled training images were created manually in GIMP 2.0 with the anchor ice portions of the surface ice filled in with gray and in the resulting images, water, frazil ice, or anchor ice were labelled 0, 1, and 2, respectively. Creating these training images was challenging because it was often difficult to distinguish visually between frazil and anchor ice pans and consequently the results are subjective. A two-group classification SVM was also used since the water in each image was neglected during training, that is, only the frazil and anchor ice superpixels were incorporated into the training matrix. The training matrix was organized the same as the surface ice training matrix, but the binary training vector contained labels for either anchor or frazil ice (i.e. 1 or 2 were used).

3.4.3 SVM Model Performance

All SVM models for predicting total ice concentration were validated by comparing predicted binary images to binary images created manually in GIMP 2.0. The fourth SVM for anchor ice delineation was validated similarly with manually labelled images distinguishing between frazil and anchor ice. Model performance was quantified using the average absolute error in concentration and the accuracy of the segmentation results using the Jaccard Index (Jaccard, 1908). These two parameters indicate the accuracy of the predicted concentration value and the segmentation

accuracy of the outputted binary image, respectively. The Jaccard Index for computing image segmentation accuracy is expressed as,

$$J(A,B) = \frac{|A \cap B|}{|A \cup B|} \tag{3.1}$$

where, A is the manually created binary image, B is the predicted binary image, $|A \cap B|$ is the intersection of the segmentation results and the manually created binary image, and $|A \cup B|$ is the union of the segmentation results and the manually created binary image. If the segmentation results exactly match that of the manually created binary image, the Jaccard Index would equal 100%.

All three models for predicting total surface ice concentrations were validated with 25 randomly chosen digital images from each respective river. Figure 3-7 shows an example of a raw digital image from the Genesee site and the corresponding binary image predicted using the appropriate model (i.e. NSR-UAV). The SVM predictions, with and without morphological operations, are compared to the four thresholding techniques in Table 3-1 and Table 3-2 using average accuracy and average absolute error, respectively. In Figure 3-8 the performance of all three surface ice concentration SVM models is illustrated by plotting the concentration predicted by the models versus the manual concentration computed from the manually created validation images. The correlation coefficients of the linear regressions plotted in Figure 3-8a-c were 0.994, 0.996, and 0.936 and the slopes of the regression lines were 1.023, 1.008, and 0.958 for the PR-UAV, NSR-UAV, and NSR-GC models, respectively, demonstrating that all three SVM models accurately predicted the total surface ice concentration.

The SVM predictions with morphological operations outperformed all four tested thresholding techniques for each of the three surface ice concentration models. Three of the thresholding methods (automated local and global thresholding and constant thresholding) gave relatively poor results with absolute errors that ranged

from 5.5% to 29.0%, and average accuracy that ranged from 37.8% to 84.1%. Manual global thresholding performed better than the other thresholding techniques and had an absolute error that ranged from 1.4% to 14.9% and an accuracy that ranged from 64.3% to 92.3%. For the images acquired at the Genesee site, manually selecting a global threshold performed similarly to the SVM and even outperformed the SVM without morphological operations. Nonetheless, this method is discouraged since it is time consuming and highly subjective. For example, there are ~28,000 game camera images of the North Saskatchewan River and manually selecting a threshold for each image would not be practical. The most accurate method was the SVM with morphological operations which had an absolute error ranging from 0.7% to 3.3% and an average accuracy or Jaccard Index that ranged from 80.1% to 93.5%.

3.5 Application of SVM Models

3.5.1 Spatial Distribution of Surface Ice Concentration

The spatial distribution of total surface ice concentration computed from UAV images at the Dunvegan Bridge boat launch on January 14, 2017 is presented in Figure 3-9. The computed surface ice concentration was very high reaching ~90% near the right bank, with lower concentrations of ~5% mid-channel, and approaching the left bank concentrations reached ~30%. Two UAV images taken near the right and left bank are presented in Figure 3-9a and Figure 3-9b, respectively. The computed spatial distribution of concentration in Figure 3-9c is consistent with these UAV images. The long white border ice formed on a small bar visible in Figure 3-9b is ignored in the computation of total surface ice concentration, because the model is not trained to identify border ice as surface ice. This application of the SVM model shows that an accurate distribution of surface ice concentration can be computed by simply flying an unmanned aerial vehicle across the width of the channel at a constant speed. This method could be further

simplified by using an unmanned aerial vehicle capable of recording position, speed, and altitude as it captures high-resolution video.

In Figure 3-10a, an oblique view UAV image of the ice conditions on the North Saskatchewan River at Genesee boat launch on December 3, 2016 is presented. In Figure 3-10b, instantaneous spatial distributions of surface ice concentrations computed every 5 seconds over ~9.5 minutes and the time-averaged spatial distribution are plotted. The instantaneous surface concentration in the center of the channel is quite variable and ranges from ~10% to 75%, whereas the surface concentration near both banks fluctuated much less. It was observed that large rafts of frazil pans (~30m diameter) were flowing in the center of the channel and a large raft can be seen entering the field of view in Figure 3-10b. The large concentration fluctuations in the center of the channel were likely due to large rafts entering and leaving the field of view of the UAV. The surface ice near the banks was generally limited to smaller individual pans that were well dispersed and this resulted in smaller fluctuations in the surface ice concentration over the 9.5 minutes.

3.5.2 Time-Series of Surface Ice Concentration

The North Saskatchewan River game camera SVM model was used to process 27,869 digital images of surface ice conditions from the bridge-mounted game cameras. There were 16,333 digital images from the game cameras deployed on the Dudley B. Menzies Bridge and 11,536 from the Fort Edmonton Footbridge between November 24 and December 7, 2016. In Figure 3-11 time-series of surface ice concentrations (10 minute and daily averaged) at each bridge are plotted along with the air temperature.

The concentration at both bridges had a similar trend leading up to December 5, 2016. On December 5th the surface concentration at the Dudley B. Menzies bridges was ~60% and in the following days it increased by ~15% each day until a solid ice cover formed on December 8, 2016. However, at the Fort Edmonton Footbridge,

the concentration remained relatively constant at ~35% between December 5 and 8, 2016 and a solid ice cover or 100% concentration was observed in the morning on December 9, 2016. Note that the ice front was observed to pass approximately one day later at the Fort Edmonton Footbridge, which is 10 km upstream of the Dudley B. Menzies Bridge.

The surface concentration at the Fort Edmonton Footbridge was significantly lower than at the Dudley B. Menzies Bridge throughout freeze-up. The difference in surface concentration between the two bridges could be due to two factors. First, the distribution of surface ice across the width of the channel is significantly different between the two bridge sites. The channel near the Dudley B. Menzies Bridge was straight and the distribution of surface ice would be relatively uniform. Near the Fort Edmonton Footbridge there is a left turning meander upstream and a large sand bar on the left bank just upstream of the bridge, and therefore the surface ice would tend to be concentrated near the right bank. This is supported by the fact that concentrations near the right bank were on average 12% higher compared to mid-channel values for the Fort Edmonton Footbridge. Second, the portion of the cross-section width captured by the game cameras at the Dudley B. Menzies Bridge was ~15% compared to ~10% at the Fort Edmonton Footbridge, respectively. In the future, additional cameras should be mounted along the length of the bridge to capture the entire cross-sectional width. This would require approximately 20 cameras on the Dudley B. Menzies Bridge and ~18 cameras on the Fort Edmonton Footbridge. Game cameras could also be deployed on a bank nearby to give some quantitative information about the spatial distribution across the width, or a UAV could be flown at various points of the year to confirm game camera observations and to obtain a spatial distribution. This type of time-series would be useful to help better estimate the amount of ice in the flow during freeze-up, and could be used to validate numerical model predictions of surface ice concentration.

3.5.3 Anchor Ice Model Performance

The SVM model for anchor ice delineation was validated with 25 images and their manually labelled images. Training images were selected from the Peace River on January 21 and 22, 2016 and January 14 and 15, 2017 when anchor ice was present in the surface ice. On January 21 and 22, 2016 the surface ice was comprised mostly of frazil ice pans with some mature anchor ice pans that had frozen over and were difficult to distinguish; this is referred to as the frazil dominated event henceforth. During the anchor ice release event that occurred on January 14 and 15, 2017 the surface ice was comprised almost exclusively of anchor ice pans (~99%); this is referred to as the anchor ice dominated event henceforth. Validation for the model was performed with 13 images from the anchor ice dominated event and 12 from the frazil dominated event. In Figure 3-12 two digital images are presented that clearly show the difference in surface ice conditions observed during the (a) frazil and (b) anchor ice dominated events.

Table 3-3 provides the predicted average anchor ice and frazil ice concentrations for the 25 validation images and the frazil and anchor ice dominated event images. The model overestimates the concentration of anchor ice and underestimates the frazil ice concentration in the frazil-dominated event images. In the anchor ice-dominated images, the model slightly overestimates the frazil ice in each image; however, the average frazil and anchor ice concentration predictions are more accurate. The average absolute error in predicted anchor and frazil ice concentrations was 5.5% and 5.6%, respectively, for all 25 validation images. Interestingly, the anchor ice dominated event images (13 of 25 validation images) were predicted with an average absolute error of 1.2% for both frazil and anchor ice predictions. The frazil dominated event images (12 of 25 validation images) were predicted with an average absolute error in predicted anchor and frazil ice concentrations of 10.2% and 7.0%, respectively. The difference in the prediction accuracy between these two events is likely due to the fact that distinguishing between two ice types when creating the validation and training images for the

frazil dominated event was very difficult and highly subjective. Conversely, it was relatively easy to distinguish between anchor ice and frazil ice pans visually when creating the validation and training images for the anchor ice dominated event, since virtually all the surface ice was comprised of anchor ice pans. This resulted in more accurate predicted concentrations for the anchor ice dominated event. A deep learning technique such as a convolution neural network could be explored in the future to try and improve these results.

3.5.4 Instantaneous Sediment Mass Flux during an Anchor Ice Release Event

The spatial distribution of surface concentration obtained for January 14, 2017, see Figure 3-9c, was used to compute an average surface concentration of 19.8%. The total surface ice concentration was comprised of virtually all anchor ice pans, so it was assumed the concentration of anchor ice was the same as the total surface ice concentration. The average instantaneous sediment mass flux, $\dot{m}$, during an anchor ice release event is given by,

$$\dot{m} = \bar{V} C_s d_f C_{AI} w (1 - \phi) \tag{3.2}$$

where, $\bar{V}$ is the average velocity, C_s is the average sediment concentration in an anchor ice pan (kg of sediment per m^3 of melt water), d_f is the average depth of an anchor ice floe, C_{AI} is the average anchor ice surface concentration, w is the width of the channel, and ϕ is the porosity of the released anchor ice. The average velocity and width at the Dunvegan Bridge were computed to be 1.31 m/s and 369 m, respectively, using the equations in Church (2015) for an average winter discharge of 1524 m^3/s. The average sediment concentration in released, floating anchor ice was found to be 28.2 g/L in a previous study by Kalke et al. (2017). Jasek (2016) measured the average depth and porosity of released anchor ice on the Peace River to be 24 cm and 0.47, respectively. Using these known parameters and the anchor ice surface concentration obtained from the SVM processed images, an

instantaneous sediment mass flux of 343 kg/s was computed for the anchor ice release event observed on the Peace River on January 14, 2017. This is within the range of instantaneous sediment mass flux computed by Kalke et al. (2017) that ranged from 0.4 to 1109 kg/s. The total annual suspended sediment load on the Peace River reported by Knight Piesold (2012) is 38,000,000 tonnes/year. This equates to an average sediment mass flux of ~1204 kg/s. However, this mass flux is likely higher during the summer months when discharges are high and lower during the winter months when discharges are low. The instantaneous sediment mass flux by anchor ice rafting of 343 kg/s is roughly one quarter of the average suspended load sediment mass flux, which means that anchor ice rafting could contribute a significant amount of sediment to a river's annual sediment budget. However, measurements of the frequency and duration of anchor ice release events over the entire winter season are needed to accurately estimate the impact that rafting by anchor ice has on the annual sediment budget.

3.6 Conclusion

Three SVMs were trained to differentiate total surface ice from water in digital images acquired with a UAV and game cameras. A fourth SVM was trained to separate the total surface ice into the frazil and anchor ice components. Four thresholding techniques, two automated and two manual techniques, were tested and compared to the SVM models that compute total surface ice concentration. The site-specific SVM models had prediction accuracies ranging from 80.1% to 93.5%, whereas thresholding techniques had prediction accuracies ranging from 37.8% to 92.3%. The absolute error in predicted concentrations ranged from 0.7% to 3.3% for the SVM models compared to a range of 1.4% to 29.0% for thresholding. The SVM models were then used to obtain a spatial distribution of ice concentration on the North Saskatchewan River at Genesee and on the Peace River at the Dunvegan Bridge boat launch, with the appropriate model. A time-series of surface concentrations was also computed from ~28,000 digital images acquired using bridge-mounted game cameras on the North Saskatchewan River at two locations.

The total surface ice concentration model for the Peace River was also used to estimate an instantaneous sediment mass flux during a release event when the surface ice was entirely comprised of anchor ice pans. These three applications of the use of site specific SVM models for estimating surface ice concentration demonstrate that this technique is a feasible, accurate and economical tool for river ice monitoring. These types of monitoring tools will help to improve our understanding of freeze-up processes and could potentially aid in the validation of numerical models.

An SVM to separate total surface ice concentration into its frazil and anchor ice components was also trained and was found to have low prediction accuracy when training images were highly subjective. That is, when it was difficult to visually distinguish between frazil and anchor ice pans. The accuracy was improved when images consisted of clearly defined anchor and frazil ice pans. A more advanced deep learning method such as a convolution neural network could be explored in future studies to separate the total surface ice into its anchor and frazil ice components. A model that is able to accurately separate frazil and anchor ice will allow for more accurate estimates of the quantity of sediment transported through anchor ice releases and could be used to compute the impact of anchor ice rafting on the annual sediment budget.

Acknowledgements

This research was supported by the Natural Sciences and Engineering Research Council of Canada (NSERC). We would like to thank Abhineet Singh and Nilanjan Ray at the University of Alberta for their assistance with the technical aspects of machine learning. Maps contained in this publication were produced by Vincent McFarlane at the University of Alberta using QGIS software (QGIS Development Team, 2017) using © OpenStreetMap data contributors (http://www.osm.org/copyright) and data obtained from AltaLIS (2017) which contains information licensed under the Open Government License – Alberta.

Figures

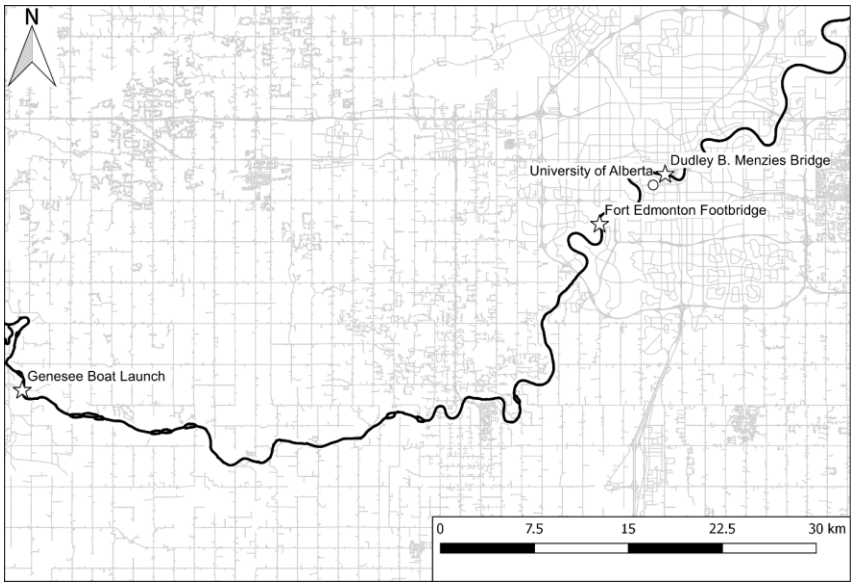

Figure 3-1. Map of the North Saskatchewan River showing the study sites (☆) in the City of Edmonton and at the Genesee boat launch.

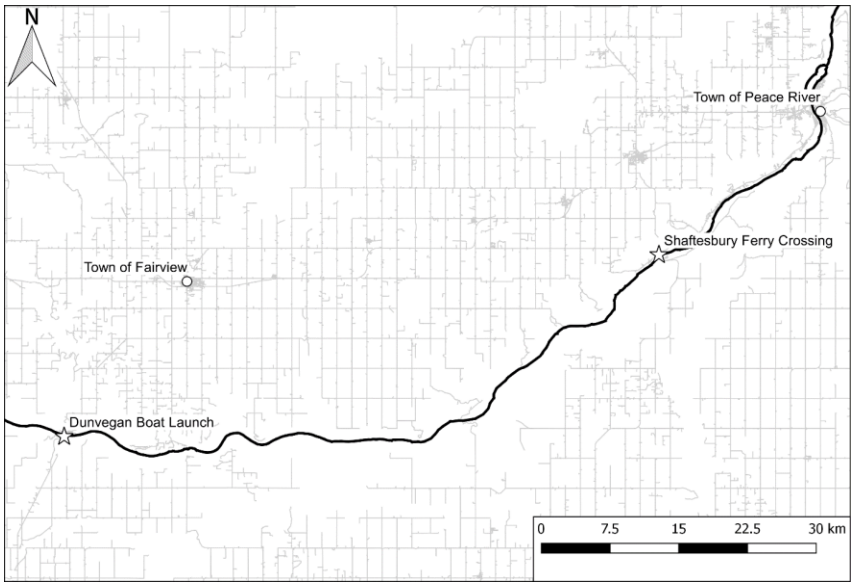

Figure 3-2. Map of the Peace River showing the study sites (☆) at the Dunvegan boat launch and Shaftesbury Ferry crossing.

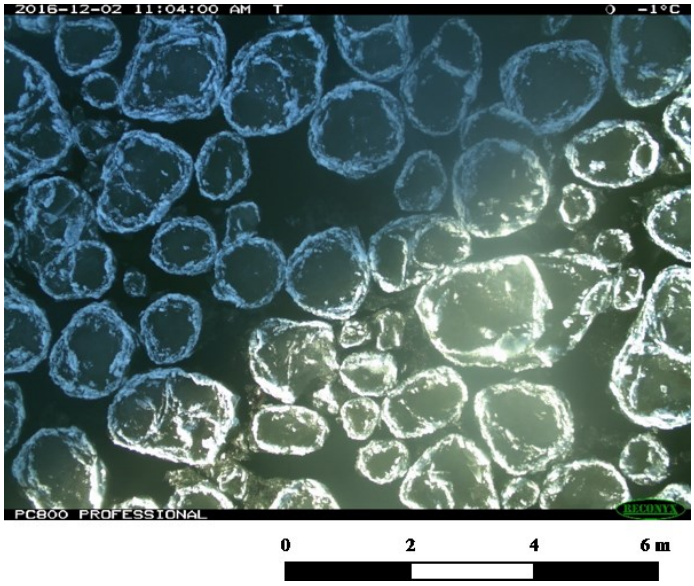

(a)

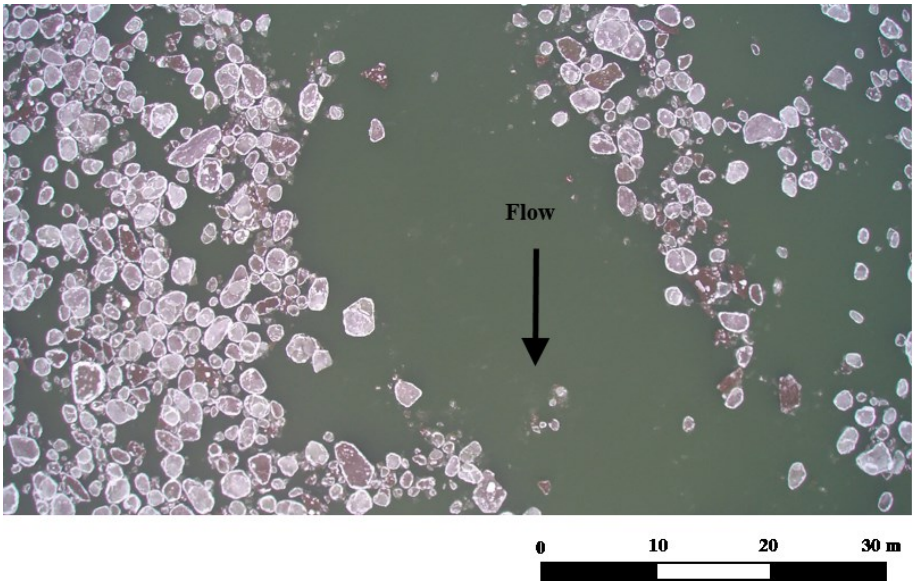

(b)

Figure 3-3. Digital image of surface ice conditions taken on (a) the North Saskatchewan River at Dudley B. Menzies Bridge on December 2, 2016 (Game Camera) and (b) the Peace River at Dunvegan Bridge on January 21, 2016 (UAV).

Figure 3-4. Digital image showing the PVC pipe game camera mount on the Fort Edmonton Footbridge. Game camera mount extends ~1.4m from the bridge railing.

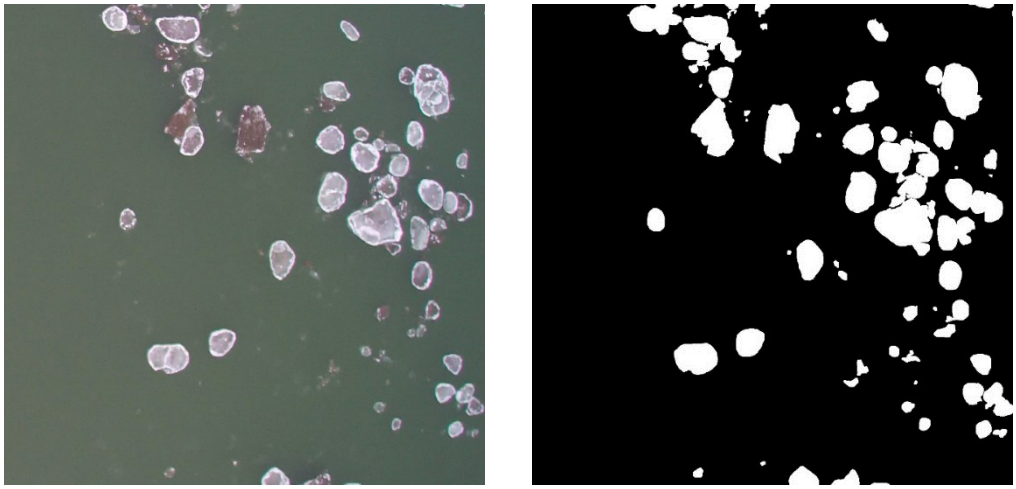

(a) (b)

Figure 3-5. Digital images provided to the SVM during training: (a) raw training image, and (b) binary training image with the surface ice delineated in white. Field of view is ~32 m wide.

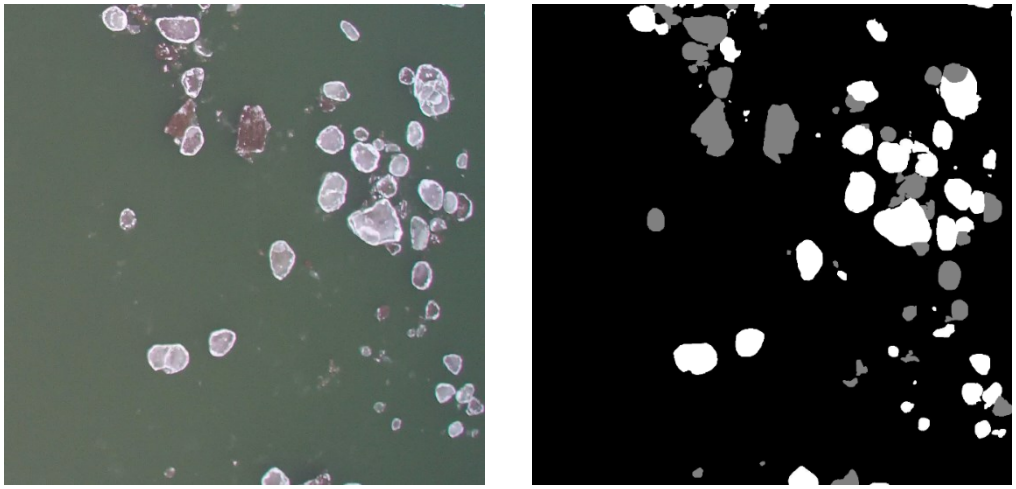

(a) (b)

Figure 3-6. Digital images provided to the anchor ice delineation SVM during training: (a) cropped raw UAV training image, and (b) labelled training image with water, anchor ice and frazil ice labelled as black, gray and white, respectively. Field of view is ~32 m wide.

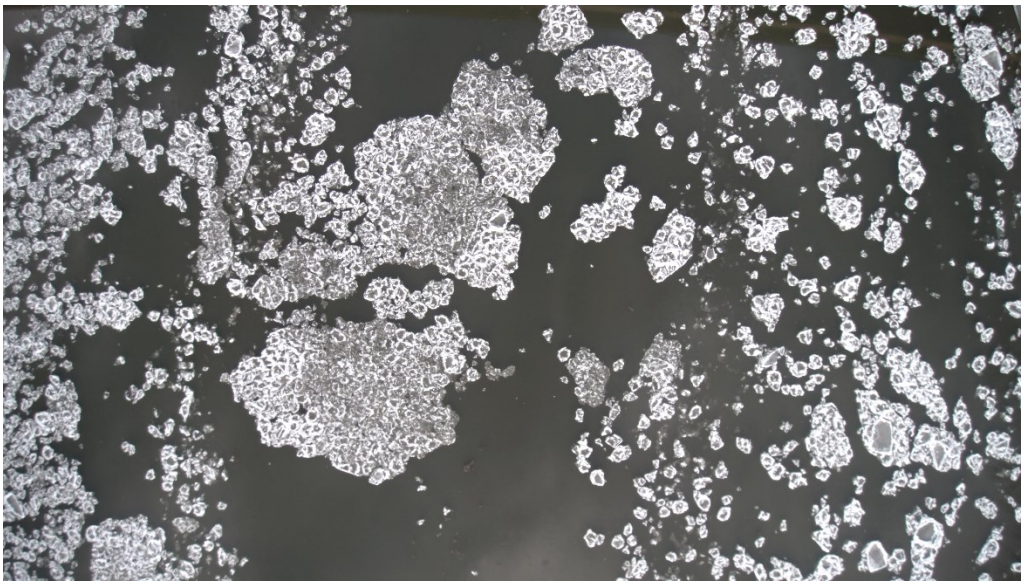

(a)

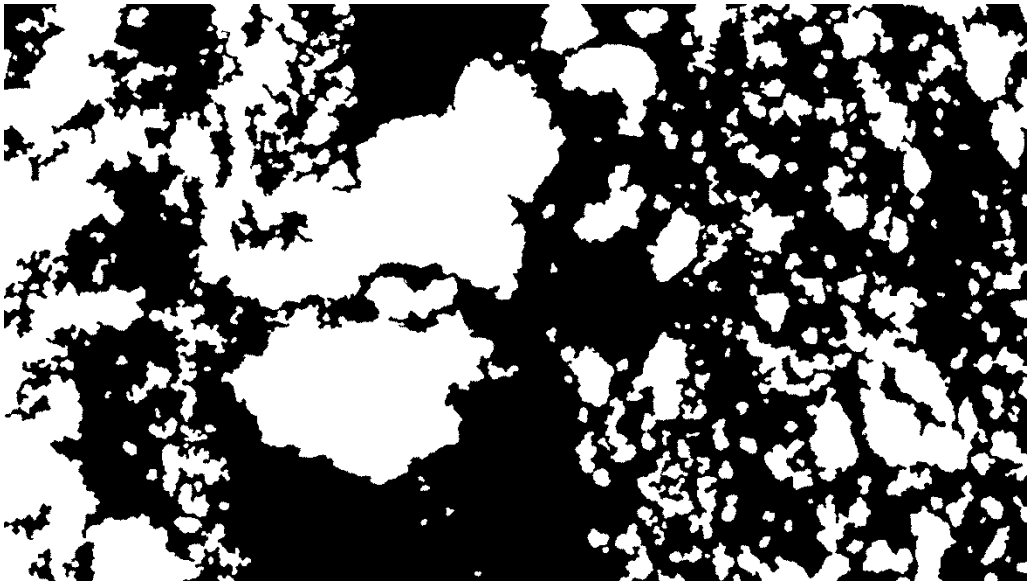

(b)

Figure 3-7. Digital images on the North Saskatchewan River at Genesee showing (a) the raw UAV captured image and (b) the predicted binary image. Field of view is ~150 m wide.

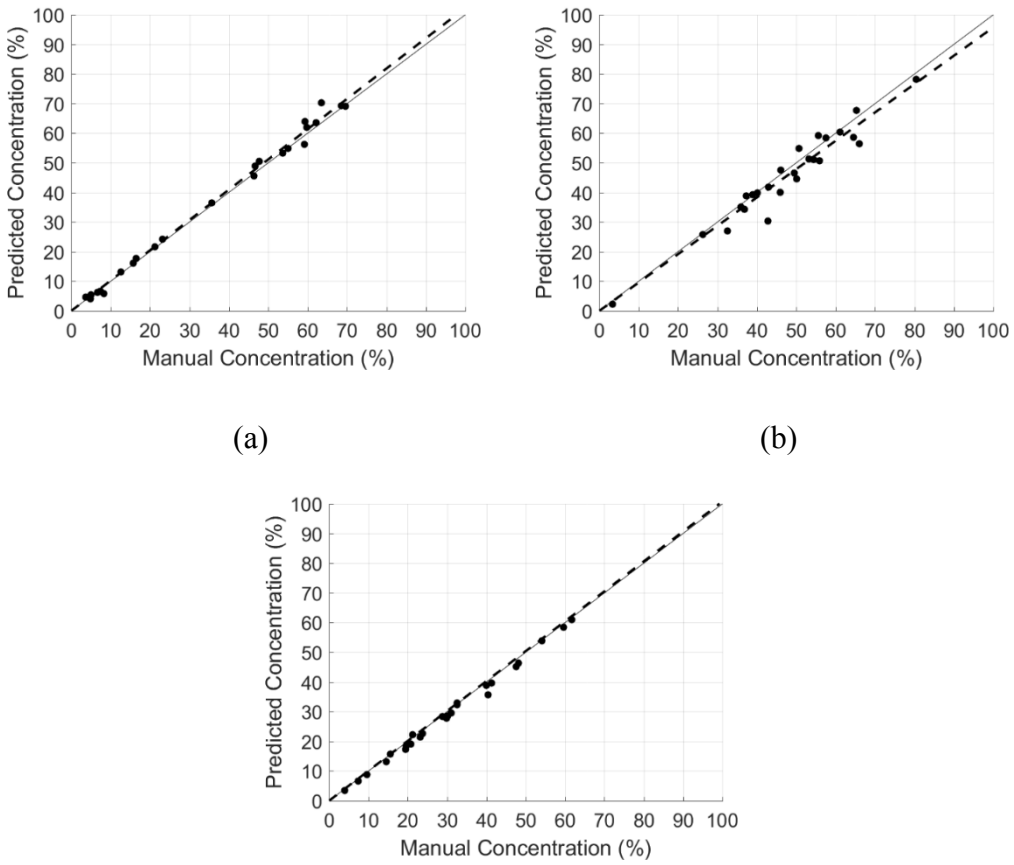

(a) (b)

(c)

Figure 3-8. Performance of the three SVMs: (a) PR-UAV model, (b) NSR-GC model, and (c) NSR-UAV model. The predicted concentrations for the 25 validation images are compared to the manual concentration obtained from manually created binary images. The dashed line is a linear regression and the solid line indicates perfect agreement.

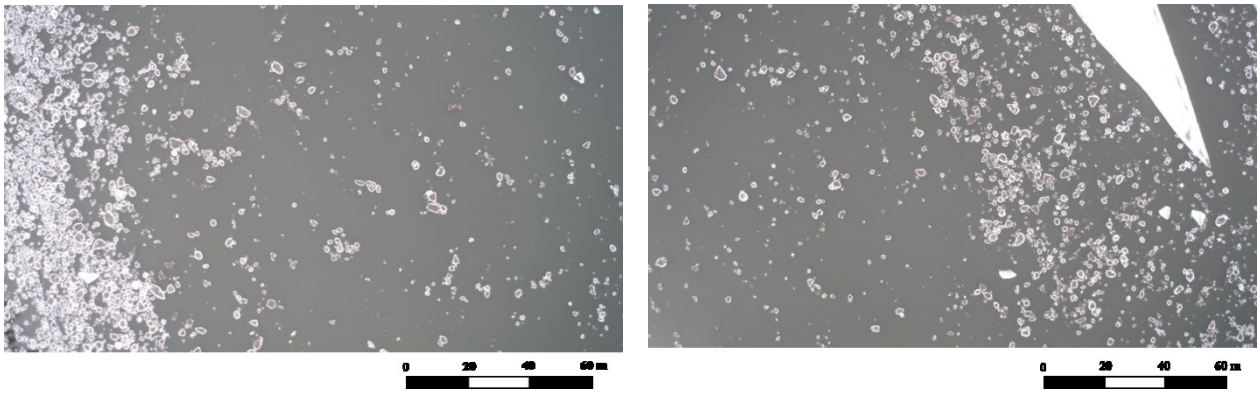

(a) (b)

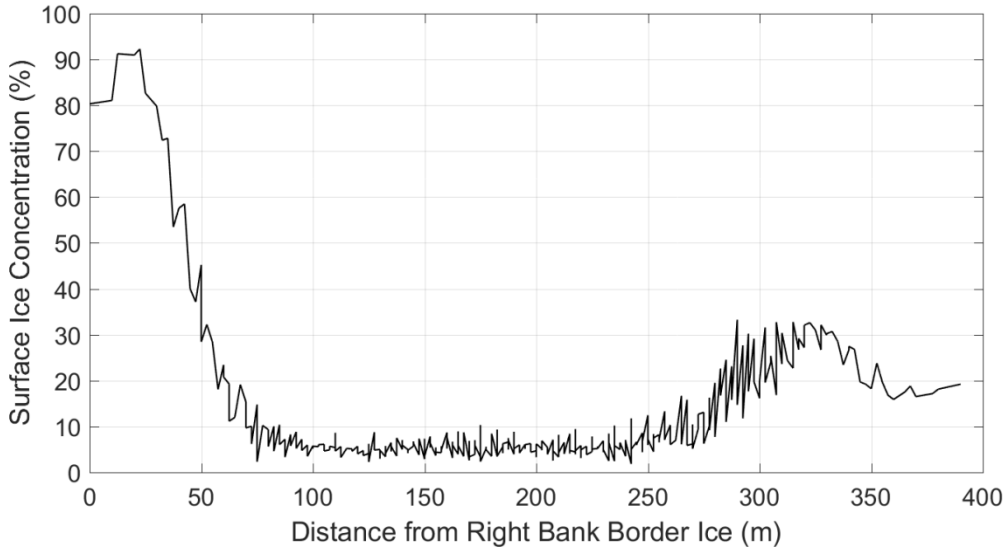

(c)

Figure 3-9. Digital images taken with the UAV showing the surface concentration at the (a) right bank and (b) left bank on January 14, 2017 at Dunvegan Bridge boat launch on the Peace River and (c) the computed spatial distribution of surface ice concentration across the channel.

(a)

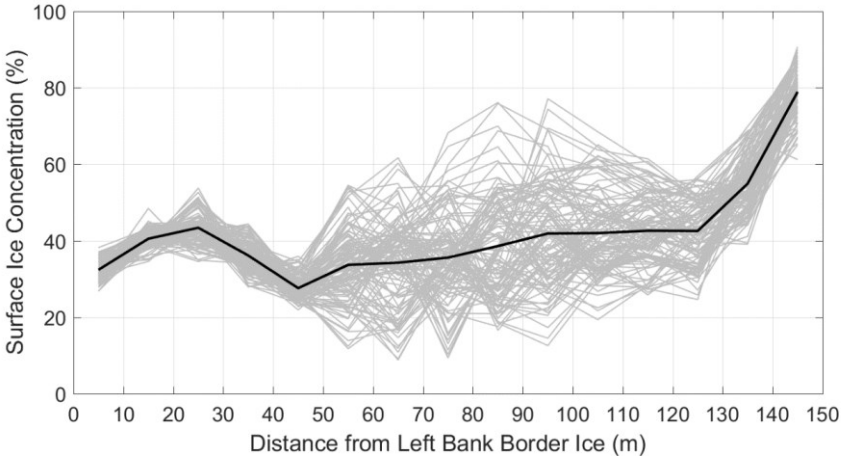

(b)

Figure 3-10. (a) Digital image taken with the UAV looking downstream showing the distribution of surface ice on December 3, 2016 at Genesee on the North Saskatchewan River (river width is ~150 m) and (b) the computed spatial distribution across the channel width. The gray lines are instantaneous concentrations at 5 second intervals and the black line is the time-averaged concentration over a ~9.5 minute duration.

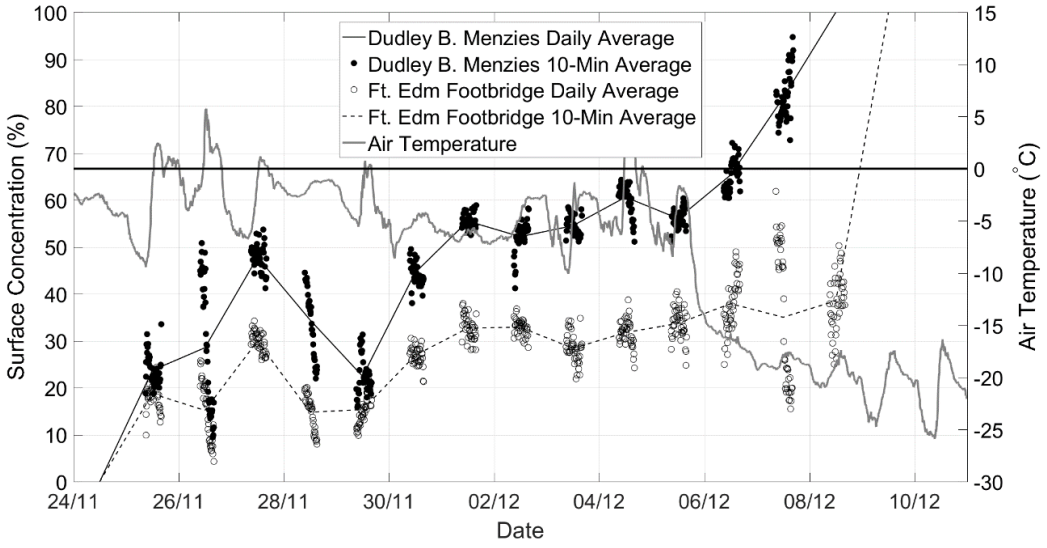

Figure 3-11. Time-series of surface ice concentration on the North Saskatchewan River at the Dudley B. Menzies Bridge and Fort Edmonton Footbridge during freeze-up between November 24 and December 8, 2016.

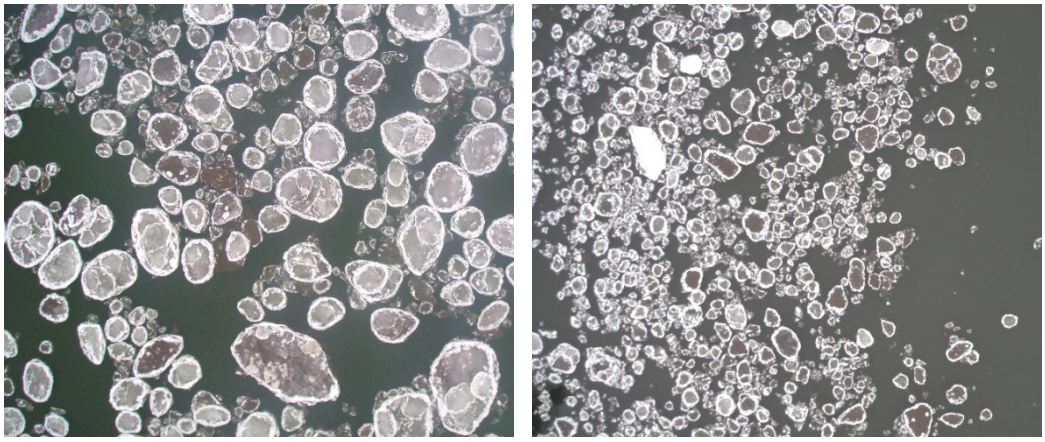

(a) (b)

Figure 3-12. Digital images showing the difference in surface ice conditions between the (a) frazil dominated event on January 21, 2016 (field of view is ~30 m wide) and (b) anchor ice dominated event on January 14, 2017 (field of view is ~60 m wide).

Tables

Table 3-1. Average accuracy (Jaccard Index) of the SVM and thresholding methods for 25 validation images.

Model	PR-UAV	NSR-GC	NSR-UAV
SVM (No Morphological Operations)	86.6%	79.1%	90.1%
SVM (Morphological Operations)	87.6%	80.1%	93.5%
Manual Global Thresholding	86.4%	64.3%	92.3%
Automated Local Thresholding (Otsu's Method)	76.2%	56.6%	78.8%
Automated Global Thresholding	63.8%	37.8%	63.5%
Constant Thresholding	64.9%	52.1%	84.1%

Table 3-2. Average absolute error in predicted surface ice concentration for the SVM and thresholding methods for 25 validation images.

Model	PR-UAV	NSR-GC	NSR-UAV
SVM (No Morphological Operations)	1.2%	4.2%	1.3%
SVM (Morphological Operations)	1.4%	3.3%	0.7%
Manual Global Thresholding	2.6%	14.9%	1.4%
Automated Local Thresholding (Otsu's Method)	7.9%	18.9%	6.5%
Automated Global Thresholding	10.0%	29.0%	11.9%
Constant Thresholding	11.9%	19.8%	5.5%

Table 3-3. Summary of the average anchor ice and frazil ice concentrations predicted for the 25 validation images and the frazil- and anchor ice-dominated event images. The manually computed concentrations are listed in brackets.

Validation Images	**Average Anchor Ice Concentration**	**Average Frazil Ice Concentration**
Frazil-Dominated	16.0% (26.3%)	26.4% (16.2%)
Anchor Ice-Dominated	18.0% (17.4%)	2.9% (3.5%)
All	17.1% (21.7%)	14.2% (9.6%)

References

Achanta, R., Shaji, A., Smith, K., Lucchi, A., Fua, P., Susstrunk, S., 2010. SLIC superpixels. EPFL Tech. Rep. 149300 15. doi:10.1109/TPAMI.2012.120

Achanta, R., Shaji, A., Smith, K., Lucchi, A., Fua, P., Süsstrunk, S., 2011. SLIC superpixels compared to state-of-the-art superpixel methods. IEEE Trans. Pattern Anal. Mach. Intell. 34, 2274–2281. doi:10.1109/TPAMI.2012.120

Alberta Environment and Parks, 2017. River ice observation report: 2016-2017 Peace River report no. 33.

Ansari, S., Rennie, C.D., Seidou, O., Malenchak, J., Zare, S.G., 2017. Automated monitoring of river ice processes using shore-based imagery. Cold Reg. Sci. Technol. 142, 1–16. doi:10.1016/j.coldregions.2017.06.011

Choisy, C., Belaid, A., 2001. Handwriting recognition using local methods for normalization and global methods for recognition, in: 6th International Conference on Document Analysis and Recognition. pp. 23–27.

Church, M., 2015. The regulation of Peace River: a case study for river management. John Wiley & Sons, Ltd., Chichester, West Sussex, UK.

Cortes, C., Vapnik, V., 1995. Support-vector networks. Mach. Learn. 20, 273–297. doi:10.1023/A:1022627411411

Jähne, B., 1997. Digital image processing, 4th ed. Springer, Germany.

Jasek, M., 2016. Investigations of anchor ice formation and release waves, in: Proceedings of the 23rd International Symposium on Ice. International Association for Hydro-Environment Envineering and Research, Ann Arbor, Michigan.

Kalke, H., Loewen, M., 2017. Predicting surface ice concentration using machine learning, in: Proceedings of the 18th Workshop on the Hydraulics of Ice Covered Rivers. Whitehorse, YT.

Kalke, H., Loewen, M., McFarlane, V., Jasek, M., 2015. Observations of anchor ice formation and rafting of sediments, in: Proceedings of the 18th Workshop on the Hydraulics of Ice Covered Rivers. Quebec City, QC.

Kalke, H., McFarlane, V., Schneck, C., Loewen, M., 2017. The transport of

sediments by released anchor ice. Cold Reg. Sci. Technol.

Kalke, H., Schneck, C., McFarlane, V., Loewen, M., Jasek, M., 2016. Ice rafting of sediment by anchor ice releases, in: Proceedings of the 22nd IAHR International Symposium on Ice. Ann Arbor, Michigan.

Kellerhals, R., Neill, C.R., Bray, D.I., 1972. Hydraulic and Geomorphic Characteristics of Rivers in Alberta. Edmonton, AB.

Kerr, D.J., Shen, H.T., Daly, S.F., 2002. Evolution and hydraulic resistance of anchor ice on gravel bed. Cold Reg. Sci. Technol. 35, 101–114.

Knight Piesold, 2012. Fluvial geomorphology and sediment transport technical data report. Vancouver, BC.

Lindenschmidt, K.-E., 2017. RIVICE—A non-proprietary, open-source, one-dimensional river-ice model. Water 9. doi:10.3390/w9050314

Osuna, E., Freund, R., Girosi, F., 1997. Training support vector machines: an application to face detection, in: IEEE Conference on Computer Vision and PAtter Recognition. Puerto Rico, pp. 130–136.

Otsu, N., 1979. A threshold selection method from gray-level histograms. IEEE Trans. Syst. Man. Cybern. 9, 62–66. doi:10.1109/TSMC.1979.4310076

Russ, J., 2007. The image processing handbook, 5th ed. CRC Press, Boca Raton, FL.

Russell, S., Norvig, P., 2010. Artificial intelligence: a modern approach, 3rd ed. Prentice Hall, Upper Saddle River, New Jersey, U.S.A.

Samuel, A., 1959. Some studies in machine learning using the game of checkers. IBM J. Res. Dev. 3, 210–229. doi:10.1147/rd.33.0210

Segaran, T., 2007. Programming collective intelligence. O'Reilly Media, Sebastopol, California.

Shen, H.T., Chen, Y.-C., Wake, A., Crissman, R., 1993. Lagrangian discrete parcel simulation of river ice dynamics, in: Proceedings of the 3rd International Offshore and Polar Engineering Conference. Singapore.

Shen, H.T., Su, J., Liu, L., 2000. SPH simulation of river ice dynamics. J. Comput. Phys. 165, 752–770. doi:10.1006/jcph.2000.6639

Tsang, G., 1982. Frazil and anchor ice: a monograph. NRC Subcommittee on

Hydraulics of Ice Covered Rivers, Ottawa, ON.

Zare, S.G.A., Ansari, S., Rennie, C.D., Seidou, O., Groeneveld, J., Ahsan, R., Malenchak, J., Ahmari, H., 2015. Simulation of river ice processes in a regulated ice covered river, in: Proceedings of the 18th Workshop on the Hydraulics of Ice Covered Rivers.

Chapter 4 Summary and Conclusions

4.1 Anchor Ice Sampling

A total of 239 anchor ice samples were obtained on three very different Albertan rivers; 204 were from released, floating anchor ice on the North Saskatchewan and Peace Rivers, whereas 35 samples were collected from anchor ice weirs on the Kananaskis River. Anchor ice samples were melted and then the total mass of sediment contained in the sample was measured after being dried at 105°C and burned at 550°C. The mean sediment concentration found in anchor ice on the North Saskatchewan, Peace, and Kananaskis Rivers were 28.1, 28.3, and 37.7 g/L, respectively. The samples collected from the Kananaskis River were significantly higher in concentration; this was attributed to collecting the samples directly from anchor ice weirs rather than from released, floating anchor ice. Therefore, the 35 samples from the Kananaskis River were excluded from the average sediment concentration in released anchor ice. The mean, median, and standard deviation of the sediment concentration contained in the 204 released anchor ice samples was found to be 28.2, 18.4, and 33.2 g/L, respectively. A lognormal distribution was observed to fit the measured sediment concentrations in anchor ice reasonably well.

Gravel and cobble size particles were also sampled from passing anchor ice and the mass and major chord length were recorded. A lognormal distribution was found to fit both the recorded mass and major chord length reasonably well for the 1,470 coarse sediment samples. The mean major chord length and mean mass of the 1,470 sampled particles were 3.6 cm and 47.7 g, respectively. This indicated that the majority of the coarse sediment moved through anchor ice was gravel sized. Another interesting finding was that 18 of the 1,470 sampled particles (1.2%) had a mass exceeding 500 g and these accounted for 24% of the total sampled mass. This shows that a small number of very coarse sediment rafted by anchor ice can significantly increase the amount of sediment transported by this process.

This study addressed the lack of available data for the sediment contained in released anchor ice on rivers, specifically for large scale rivers such as the Peace and North Saskatchewan River. This will ultimately lead to a better understanding of the contribution anchor ice has on the annual sediment budget for these rivers.

4.2 Support Vector Machine Image Processing

Digital images of surface ice conditions were acquired using bridge-mounted game cameras and an unmanned aerial vehicle (UAV). Surface ice concentration was computed by using image processing algorithms to convert the original raw digital image to a binary image separating the total surface ice from the water. Three support vector machines (SVMs) were trained to create a binary image from a raw digital image that separates the total surface ice from water. Four thresholding techniques, two manual and two automated, were also used and were compared to the results of the three SVM models. The predicted surface ice concentration for each image processing technique was compared to the concentration computed from manually created binary images using photo-editing software. The SVM models outperformed the thresholding techniques and were found to be between 1.2% and 42.3% more accurate for computing surface ice concentration. The site-specific SVM models had prediction accuracies ranging from 80.1% to 93.5%, whereas thresholding had prediction accuracies ranging from 37.8% to 92.3%. The absolute error in predicted concentrations ranged from 0.7% to 3.3% for the site specific SVMs, whereas thresholding gave an absolute error of 1.4% to 29.0%.

The highly accurate SVM models were then used to compute a spatial distribution of concentration on the Peace and North Saskatchewan Rivers and a time-series of surface concentrations during freeze-up in the City of Edmonton on the North Saskatchewan River. On the Peace River, the channel width was too large (~400m) to be captured entirely by the UAV camera. The maximum permissible height the UAV can be flown is ~90 m, which equates to roughly 180 m of river width captured in the image. Digital images across the channel were obtained by flying

the drone at a constant speed from the left to right bank. The images acquired from the UAV across the channel were processed with the appropriate SVM and a spatial distribution was plotted. Another method for plotting the spatial distribution was to fix the UAV above the center of channel so that the entire channel is captured in the digital image. This could be done on the North Saskatchewan River at Genesee where the river width is ~150 m. A spatial distribution was plotted every 5 seconds over a ~9.5-minute duration, and an average surface concentration over this duration was also plotted. This allowed for an accurate representation of the average surface ice concentration across the channel since the random fluctuations from large frazil rafts were normalized. A time-series of surface ice concentrations during freeze-up was also computed on the North Saskatchewan River and plotted as 10-minute and daily averages. This time-series was computed from ~28,000 digital images captured on the North Saskatchewan River from bridge-mounted game cameras between November 24 and December 8, 2016. The trained site-specific SVM models presented in this study to estimate total surface ice concentration will assist in computing surface ice concentration in future studies with additional digital images acquired during freeze-up. This will help to improve our understanding of freeze-up processes and could potentially aid in the validation of numerical models.

An SVM to separate total surface ice concentration into its frazil and anchor ice components was also trained and was found to have low prediction accuracy when training images were highly subjective. On the Peace River on January 21 and 22, 2016, digital images of surface ice were a mix of both frazil and anchor ice. The anchor ice in these images was difficult to distinguish since they had developed a solid frozen cover and upturned white edges that was similar to the appearance of the frazil ice pans. This subjectivity in both the training and validation images make it difficult for the model to produce accurate results. If there is significant erroneous data in the training matrix, the model will be unable to find an accurate separating hyperplane. This was supported by digital images on January 14, 2017 where the anchor ice and frazil ice was easily separable and the model computed anchor and

frazil ice concentrations within 1.2% on average. A deep learning model such as a convolution neural network could be explored in future studies to separate the total surface ice into its anchor and frazil ice components when digital images are very subjective. A model that is able to accurately separate frazil and anchor ice will allow for more accurate estimates of the quantity of sediment transported through anchor ice releases. These estimates could then be used with digital images acquired over an entire winter season to compute the impact of anchor ice rafting on the annual sediment budget.

4.3 Recommendations for Future Research

Additional digital imagery should be obtained on the Peace River where there is a significant amount of anchor ice released throughout the winter season. Game cameras could be deployed across the length of the Dunvegan Bridge and pointed parallel with the water surface. These cameras should be deployed to give sufficient coverage of the river width, and UAV flights should be performed at various times to confirm the spatial distribution. An automated model that can compute the anchor ice concentration in the flow will allow for better estimates of the total quantity of sediment transported through anchor ice over a winter season. Therefore, a deep learning method should be explored to try and separate frazil and anchor ice in the total surface ice when digital images are highly subjective. This would aid in image processing and computation of anchor ice surface concentration if game cameras are deployed along the Dunvegan Bridge.

Additional measurements of released anchor ice should be taken to aid in understanding the impact of anchor ice sediment transport; these include the average depth of each pan and average porosity. Additional field measurements of the sediment contained in anchor ice could also be collected before and during release events to provide insight into the impact of the release mechanism (i.e. thermal or mechanical) on the size of sediment transported by anchor ice. Bed

samples should be collected during sampling to determine if the size distribution is impacted by local bed size or by release mechanism.

Advancing our theoretical understanding of anchor ice formation and release would be also helpful to better quantify the amount of sediment transported through this process. A key advance would be the development of more accurate equations for predicting how much of the suspended frazil that is generated in the water column rises to the surface and how much is deposited on the bed forming anchor ice. Additionally, accurate methods for computing the growth rate of anchor ice through both frazil deposition and in-situ crystal growth are needed in order to estimate the quantity of anchor ice in a river at a given time. Furthermore, understanding how anchor ice releases through both thermal and mechanical mechanisms and what parameters govern each type of release (i.e. water temperature, ambient air temperature, the movement of the zero-degree isotherm, channel velocity, etc.) are needed to predict the surface concentration of anchor ice pans.

References

Achanta, R., Shaji, A., Smith, K., Lucchi, A., Fua, P., Susstrunk, S., 2010. SLIC superpixels. EPFL Tech. Rep. 149300 15. doi:10.1109/TPAMI.2012.120

Achanta, R., Shaji, A., Smith, K., Lucchi, A., Fua, P., Süsstrunk, S., 2011. SLIC superpixels compared to state-of-the-art superpixel methods. IEEE Trans. Pattern Anal. Mach. Intell. 34, 2274–2281. doi:10.1109/TPAMI.2012.120

Alberta Environment and Parks, 2017. River ice observation report: 2016-2017 Peace River report no. 33.

Ansari, S., Rennie, C.D., Seidou, O., Malenchak, J., Zare, S.G., 2017. Automated monitoring of river ice processes using shore-based imagery. Cold Reg. Sci. Technol. 142, 1–16. doi:10.1016/j.coldregions.2017.06.011

Choisy, C., Belaid, A., 2001. Handwriting recognition using local methods for normalization and global methods for recognition, in: 6th International Conference on Document Analysis and Recognition. pp. 23–27.

Church, M., 2015. The regulation of Peace River: a case study for river management. John Wiley & Sons, Ltd., Chichester, West Sussex, UK.

Cortes, C., Vapnik, V., 1995. Support-vector networks. Mach. Learn. 20, 273–297. doi:10.1023/A:1022627411411

Daly, S., 1994. Report on frazil ice. Hanover, New Hampshire.

Dayton, P.K., Robilliard, G., Devries, A.L., 1969. Anchor ice formation in McMurdo Sound, Antarctica. American Association for the Advancement of Science, Washington, D.C.

Doering, J., Bekeris, L., Morris, M., Dow, K., Girling, W., 2001. Laboratory Study of anchor ice growth. J. Cold Reg. Eng. 15, 60–66.

Emmer, S., Nafziger, J., McFarlane, V., Loewen, M., Hicks, F., 2013. Winter Ice Processes of the Kananaskis River, Alberta, in: Proceedings of the 17th Workshop on River Ice. Committee on River Ice Processes and the Environment, Edmonton, AB.

Girling, W., Groeneveld, J., 1999. Anchor ice formation below Limestone Generating Station. Manitoba Hydro, Winnipeg, MN.

Gosink, J., Osterkamp, T., 1986. Frazil ice nucleation by ejecta from supercooled water, in: Proceedings of the 8th IAHR Symposium on Ice. Iowa City, Iowa, pp. 249–263.

Hirayama, K., Terada, K., Sato, M., Hirayama, K., Sasamoto, M., Yamazaki, M., 1997. Field measurements of anchor and frazil ice, in: Proceedings of the 9th Workshop on River Ice. Fredericton, NB.

Jähne, B., 1997. Digital image processing, 4th ed. Springer, Germany.

Jasek, M., 2016. Investigations of anchor ice formation and release waves, in: Proceedings of the 23rd International Symposium on Ice. International Association for Hydro-Environment Envineering and Research, Ann Arbor, Michigan.

Jasek, M., Shen, H.T., Pan, J., Paslawski, K., 2015. Anchor ice waves and their impact on winter ice cover stability, in: Proceedings of the 18th Workshop on the Hydraulics of Ice Covered Rivers. Quebec City, QC.

Kalke, H., Loewen, M., 2017. Predicting surface ice concentration using machine learning, in: Proceedings of the 18th Workshop on the Hydraulics of Ice Covered Rivers. Whitehorse, YT.

Kalke, H., Loewen, M., McFarlane, V., Jasek, M., 2015. Observations of anchor ice formation and rafting of sediments, in: Proceedings of the 18th Workshop on the Hydraulics of Ice Covered Rivers. Quebec City, QC.

Kalke, H., McFarlane, V., Schneck, C., Loewen, M., 2017. The transport of sediments by released anchor ice. Cold Reg. Sci. Technol.

Kalke, H., Schneck, C., McFarlane, V., Loewen, M., Jasek, M., 2016. Ice rafting of sediment by anchor ice releases, in: Proceedings of the 22nd IAHR International Symposium on Ice. Ann Arbor, Michigan.

Kellerhals, R., Neill, C.R., Bray, D.I., 1972. Hydraulic and Geomorphic Characteristics of Rivers in Alberta. Edmonton, AB.

Kempema, E., Ettema, R., 2011. Anchor ice rafting: observations from the Laramie River. River Res. Appl. 27, 1126–1135.

Kempema, E., Ettema, R., McGee, B., 2008. Insights from anchor ice formation in the Laramie River, Wyoming, in: Proceedings of the 19th International

Symposium on Ice. Vancouver, BC.

Kempema, E.W., Reimnitz, E., Barnes, P.W., 2001. Anchor-ice formation and ice rafting in southwestern Lake Michigan, U.S.A. J. Sediment. Res. 71, 346–354. doi:10.1306/2DC40948-0E47-11D7-8643000102C1865D

Kempema, E.W., Reimnitz, E., Clayton, J.R., Payne, J.R., 1993. Interactions of frazil and anchor ice with sedimentary particles in a flume. Cold Reg. Sci. Technol. 21, 137–149.

Kempema, E.W., Reimnitz, E., Hunter, R.E., 1986. Flume studies and field observations of the interaction of frazil ice and anchor ice with sediment. U.S. Geological Survey, Menlo Park, California.

Kerr, D.J., Shen, H.T., Daly, S.F., 1997. Anchor ice formation and growth on gravel channel bed, in: Proceedings of the 9th Workshop on River Ice. Fredericton, NB.

Kerr, D.J., Shen, H.T., Daly, S.F., 2002. Evolution and hydraulic resistance of anchor ice on gravel bed. Cold Reg. Sci. Technol. 35, 101–114.

Knight Piesold, 2012. Fluvial geomorphology and sediment transport technical data report. Vancouver, BC.

Lindenschmidt, K.-E., 2017. RIVICE—A non-proprietary, open-source, one-dimensional river-ice model. Water 9. doi:10.3390/w9050314

Nafziger, J., She, Y., Hicks, F., Cunjak, R.A., 2017. Anchor ice formation and release in small regulated and unregulated streams. Cold Reg. Sci. Technol. 141, 66–77. doi:10.1016/j.coldregions.2017.05.008

Osterkamp, T.E., 1978. Frazil Ice Formation: A Review. J. Hydraul. Div.

Osuna, E., Freund, R., Girosi, F., 1997. Training support vector machines: an application to face detection, in: IEEE Conference on Computer Vision and PAtter Recognition. Puerto Rico, pp. 130–136.

Otsu, N., 1979. A threshold selection method from gray-level histograms. IEEE Trans. Syst. Man. Cybern. 9, 62–66. doi:10.1109/TSMC.1979.4310076

Qu, Y.X., Doering, J., 2007. Laboratory study of anchor ice evolution around rocks and on gravel beds. Can. J. Civ. Eng. 34, 46–55.

Russ, J., 2007. The image processing handbook, 5th ed. CRC Press, Boca Raton,

FL.

Russell, S., Norvig, P., 2010. Artificial intelligence: a modern approach, 3rd ed. Prentice Hall, Upper Saddle River, New Jersey, U.S.A.

Samuel, A., 1959. Some studies in machine learning using the game of checkers. IBM J. Res. Dev. 3, 210–229. doi:10.1147/rd.33.0210

Segaran, T., 2007. Programming collective intelligence. O'Reilly Media, Sebastopol, California.

Shen, H.T., Chen, Y.-C., Wake, A., Crissman, R., 1993. Lagrangian discrete parcel simulation of river ice dynamics, in: Proceedings of the 3rd International Offshore and Polar Engineering Conference. Singapore.

Shen, H.T., Su, J., Liu, L., 2000. SPH simulation of river ice dynamics. J. Comput. Phys. 165, 752–770. doi:10.1006/jcph.2000.6639

Smedsrud, L., 2001. Frazil-ice entrainment of sediment : large-tank laboratory experiments. J. Glaciol. 47, 461–471.

Stickler, M., Alfredsen, K., 2009. Anchor ice formation in streams: a field study. Hydrol. Process. 23, 2307–2315.

Terada, K., Hirayama, K., Sasamoto, M., 1998. Field Measurements of Anchor and Frazil Ice, in: Proceedings of the 14th International Symposium on Ice. International Association for Hydro-Environment Envineering and Research, Potsdam, NY.

Tremblay, P., Leconte, R., Jay Lacey, R.W., Bergeron, N., 2014. Multi-day anchor ice cycles and bedload transport in a gravel-bed stream. J. Hydrol. 519, 364–375.

Tsang, G., 1982. Frazil and anchor ice: a monograph. NRC Subcommittee on Hydraulics of Ice Covered Rivers, Ottawa, ON.

Wigle, T.E., 1970. Investigations into frazil, bottom ice and surface ice formation in the Niagara River, in: Proceedings of the 1st International Symposium on Ice. International Association for Hydro-Environment Envineering and Research, Reykjavik, Iceland.

Yamazaki, M., Hirayama, K., Sakai, S., Sasamoto, M., Kiyohara, M., Takiguchi, H., 1996. Formation of frazil and anchor ice, in: Proceedings of the 13th

International Symposium on Ice. International Association for Hydro-Environment Envineering and Research, Beijing, China.

Ye, S.Q., Doering, J., Shen, H.T., 2004. A laboratory study of frazil evolution in a counter- rotating flume. Can. J. Civ. Eng. 31, 899–914. doi:10.1139/L04-056

Zare, S.G.A., Ansari, S., Rennie, C.D., Seidou, O., Groeneveld, J., Ahsan, R., Malenchak, J., Ahmari, H., 2015. Simulation of river ice processes in a regulated ice covered river, in: Proceedings of the 18th Workshop on the Hydraulics of Ice Covered Rivers.

Appendix A. Description of MATLAB Codes for SVM Image Processing

Program Name	Description
SVM_Training.m	Builds training matrix and binary training vector and then trains a support vector machine classifier.
SVM_Predict.m	Builds input matrix for new digital images and uses trained support vector machine to predict new binary images
AI_Training.m	Builds training matrix and training vector and then trains a support vector machine classifier for anchor ice delineation.
AI_Prediction.m	Builds input matrix for new digital images and uses trained support vector machine to predict new labelled images for anchor ice delineation.
Frame_Extractor.m	Extracts digital images from continuous UAV video at set intervals.
Jaccard_Index.m	Loads predicted binary images from SVM and thresholding to compute the Jaccard Index and average absolute error.